This article is published as part of the *Dalton Transactions* themed issue entitled:

Molecular Magnets

Guest Editor Euan Brechin
University of Edinburgh, UK

Published in issue 20, 2010 of *Dalton Transactions*

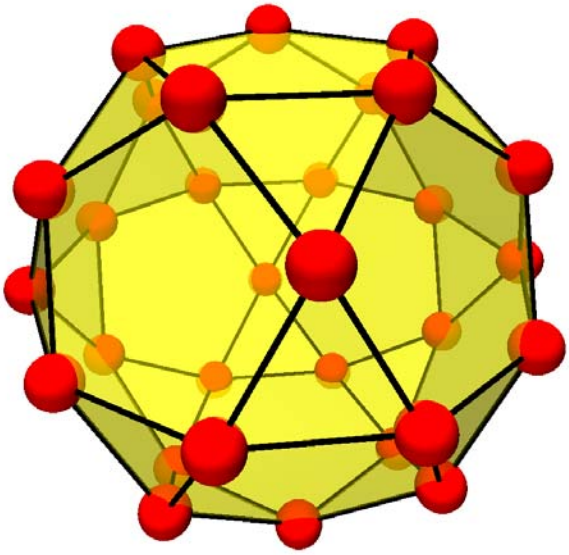

Image reproduced with permission of Jürgen Schnack

Articles in the issue include:

PERSPECTIVES:

COMMUNICATIONS:

Rational design of covalently bridged [$Fe^{III}_2M^{II}O$] clusters†

Pablo Alborés*[a,b] and Eva Rentschler*[a]

Received 2nd December 2009, Accepted 28th January 2010
First published as an Advance Article on the web 5th March 2010
DOI: 10.1039/b925214b

We are reporting the first supramolecular dimeric units of basic carboxylates. The neutral [$Fe^{III}_2M^{II}O$] motif for different 3d M metals is covalently bound through 2,2′-bipyrimidine. We have structurally characterized the hexanuclear clusters and the related trinuclear building blocks. Their magnetic properties have been fully analyzed and DFT calculations have been performed as a supplementary tool. All results evidence a weak antiferromagnetic interaction through the bpym bridge between isolated spin ground states (in some examples) arising from intra-Fe_2MO core exchange couplings.

Introduction

Molecular clusters of 3d transition metals continue to be of major interest in the research due to their fascinating physical properties and their complex structures. In particular, they often show high-spin ground states and easy axis-type magnetic anisotropy, giving a significant energy barrier to reversal of the magnetization. Thus, at sufficiently low temperatures they behave as nanoscale single domain magnets.[1] Such single-molecule magnets (SMMs) span the classical/quantum interface by displaying not just classical magnetization hysteresis but also quantum tunneling of magnetization (QTM)[2] and quantum phase interference.[3] SMMs represent a molecular, or "bottom-up", route to nanoscale magnetic materials,[4] with potential applications in information storage and spintronics[5,6] at the molecular level and use as quantum bits (qubits) in quantum computation.[5,7] Regarding the latter, it has been shown that SMM properties are not essential requisites for transition metal clusters suitability within the quantum computation research area. A cluster size big enough to make addressing possible and an isolated spin ground state are the starting essential features.[5] Magnetic molecules have been proposed as a novel route to a spin-based implementation of quantum-information processing.[7,8]

Within this field, the assembly of pre-formed polymetallic clusters by covalent bonds in a step-by-step strategy has become quite a desirable goal for chemists. As an example, the linking of SMM in a rational manner was only introduced a few years ago.[9] Since then, this procedure has opened the way to 1D–3D frameworks that exhibit properties ranging from classical to quantum magnetism.[10-12] However, very few examples have been reported of discrete covalently attached 3d transition metal clusters and even less examples of a rational strategy have been employed.[13] The very recently reported Cr_7Ni covalently attached wheels appear as the out-standing example of well characterized rational assembled molecular clusters, where the properties of the building unit can be separately studied and understood.[14]

The "basic carboxylate", [$M_3O(O_2CR)_6$] (with M a first row d-block transition metal and R a suitable organic group) core, known for a couple of decades,[15] is a good starting reagent in the preparation of clusters with higher nuclearity. The most prominent example being the synthesis of the pioneer SMM, $Mn_{12}O_{12}(O_2CR)_{16}(H_2O)_4$.[16] In spite of this, there are only a few examples reported to date where this μ_3-O core is used as a "true" building block for the construction of supramolecular arrangements, specifically by linking them with appropriate bridging units through covalent bonds.[11,12,17] However, all these examples are extended systems and no reports can be found of discrete molecular species where two or more M_3O units are connected for 3d metals. The only well known examples are the covalent linked Ru_3O basic carboxylate cores, prepared in a rather rational approach.[18]

We are reporting here, the first example of supramolecular dimeric units of basic carboxylates baring the neutral $Fe^{III}_2M^{II}O$ motif for different 3d M metals, covalently linked by the tetradentate 2,2′-bipyrimidine ligand (bpym). We have structurally characterized these hexanuclear clusters and the related trinuclear building blocks. Their magnetic properties have been fully analyzed and DFT calculations have been performed as

[a]*Institute of Inorganic and Analytical Chemistry, Johannes Gutenberg - University of Mainz, Duesbergweg 10-14, D-55128 Mainz, Germany. E-mail: albores@qi.fcen.uba.ar, rentschl@uni-mainz.de; Fax: +49 6131/39-23922*

[b]*Departamento de Química Inorgánica, Analítica y Química Física, INQUIMAE (CONICET), Facultad de Ciencias Exactas y Naturales Universidad de Buenos Aires, Pabellón 2, Ciudad Universitaria, C1428EHA Buenos Aires, Argentina; Fax: +5411/4576-3341*

† Electronic supplementary information (ESI) available: Fig. S1: molecular representation of the H-bonding between adjacent molecules in complex **1**; Fig. S2: arrangement of the H-bond interacting complexes in the crystal packing of **1**; Fig. S3: molecular representation of the extended H-bond interaction in complex **4**; Fig. S4: crystal packing of the unit cell of complex **4**; Fig. S5: molecular representation of the extended H-bond interaction in complex **6**; Fig. S6: crystal packing of the unit cell of complex **6**; Fig. S7: overlaid X-ray structures of the pair complexes **1–4**, **2–5** and **3–6**; Fig. S8: overlaid Mössbauer spectra at 80 K of complexes **4**, **5** and **6**; Fig. S9: overlaid $\chi_m T$ data plots of the complexes pairs **1–4**, **2–5** and **3–6**; Fig. S10: spin density isosurfaces of the different spin topologies employed in the broken-symmetry exchange coupling constants calculations of complexes **1–3** (illustrated with compound **2**); Fig. S11: spin density isosurfaces of the different spin topologies employed in the broken-symmetry exchange coupling constants calculations of complexes **4–6** (illustrated with compound **5**); Fig. S12: natural localized orbitals pairs with unitary occupancy, centered at Co(II) sites that show σ-type exchange pathway through the bipyrimidine bridge in complex **4**; Fig. S13: natural localized orbitals pairs with unitary occupancy, centered at Fe(III) sites, that show σ-type exchange pathway through the bipyrimidine bridge in complex **6**. CCDC reference numbers 750190–750195. For ESI and crystallographic data in CIF or other electronic format see DOI: 10.1039/b925214b

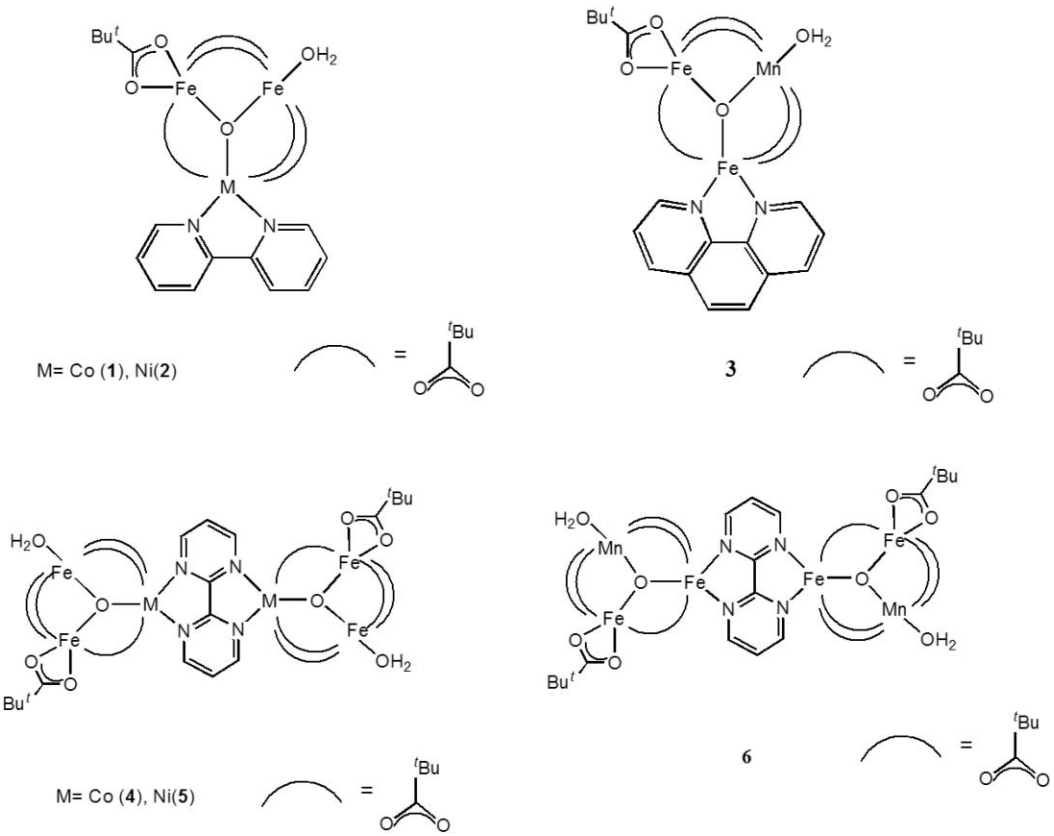

Scheme 1 Pictorial sketch of the reported new complexes **1–6**.

a supplementary tool. All results evidence a weak interaction through the bpym bridge between isolated spin ground states arising from intra-Fe_2MO core exchange couplings.

Results and discussion

Synthesis

The well proven synthetic versatility of the μ_3-oxo triangular iron basic carboxylate precursor, $[Fe_3O(RCOO)_6L_3]^+$ (L = neutral ligand), prompted us to use it as the building block for constructing higher nuclearity clusters in a rational approach. Taking advantage of the relative stability of the heteronuclear $[Fe^{III}{}_2M^{II}\text{-}\mu_3O]$ core and the driving force of its neutral character regarding crystallization properties, we studied the reaction of $[Fe_3O(O_2C^tBu)_6(H_2O)_3]ClO_4$ in acetonitrile with a M(II) source in the presence of the bidentate ligand 2,2′-bipyridine (bpy) or 1,10′-phenantroline (phen). Single crystals obtained under smooth conditions proved that the final product is still a triangular core but now incorporating one M(II) in place of one Fe(III), which additionally appears as the preferred coordination site for the bpy ligand. In view of the two-site coordination mode of the latter, one of the μ_2 bridging carboxylates in the starting precursor changes to a non-bridging κ^2-O, O′ mode and two of the apical H_2O ligands are removed (Scheme 1). Interestingly, a different product is obtained when M is Mn^{2+}. Here the bidentate ligand 1,10′- phenantroline (phen) is not coordinated to the Mn(II) site but to the Fe(III) one. This behaviour suggests that both high-spin d^5 configurations of Mn(II) and Fe(III) do not show strong preference for the phen ligand.

Once the synthetic route is well established, it is possible to replace the bidentate ligand bpy by the parent tetradentate, 2,2′-bipyrimidine (bpym). Under the same reaction conditions but adjusting the stoichiometric relationship in order to have a 2 : 1 ratio between the Fe_3O precursor and the bpym ligand, neutral hexanuclear $[(Fe^{III}{}_2M^{II}O)\text{-}\mu(bpym)\text{-}(Fe^{III}{}_2M^{II}O)]$ products are obtained as confirmed by single crystal X-ray crystallography. Noticeably they are built up of exactly bpym bridged, compounds **1–3** (Scheme 1) where the bpy leaves its place to the bpym, evidencing the success of this rational approach. In all cases, analytical pure single crystals are directly obtained from the reaction, aided by their poor solubility in acetonitrile.

Crystal and molecular structures

All triangular complexes **1–3** are isomorphous and crystallize in a triclinic cell, space group $P\bar{1}$ (Table 1). Each unit cell contains two neutral complex molecules, and two acetonitrile solvent molecules. The complex molecules are interacting trough H-bonds between the coordinated aqua ligand and two pivalate oxygen atoms from the neighbour molecule, holding the closest inter-molecular metal–metal distance at about 5 Å (see ESI†). The bulky *tert*-butyl groups keep those formed pairs well isolated from each other. The molecular structures show the planar $[Fe^{III}{}_2M\text{-}\mu_3O]$ motif typically observed in basic carboxylates but in this case with only five μ_2 complementary carboxylate bridges instead of six (Fig. 1). The sixth carboxylate adopts a κ^2-O,O′ non-bridging coordination mode leaving one free site for the bidentate ligand coordination at the neighbouring metal ion. The apical position at the remaining

Table 1 Crystallographic data and refinement parameters

	1	2	3	4	5	6
Formula	$C_{42}H_{67}CoFe_2N_3O_{14}$	$C_{42}H_{67}Fe_2N_3NiO_{14}$	$C_{44}H_{67}Fe_2MnN_3O_{14}$	$C_{72}H_{124}Co_2Fe_4N_6O_{28}$	$C_{72}H_{124}Fe_4N_6Ni_2O_{28}$	$C_{76}H_{130}Fe_4Mn_2N_8O_{28}$
Formula weight	1008.62	1008.40	1028.65	1863.03	1862.59	1937.16
T/K	173	173	173	173	173	173
Wavelength/Å	0.71073	0.71073	0.71073	0.71073	0.71073	0.71073
Crystal system	Triclinic	Triclinic	Triclinic	Triclinic	Triclinic	Monoclinic
Space group	$P\bar{1}$	$P\bar{1}$	$P\bar{1}$	$P\bar{1}$	$P\bar{1}$	$P21/n$
a/Å	11.4643(4)	11.4460(7)	11.5312(7)	11.8218(10)	11.7753(4)	14.6170(16)
b/Å	12.0792(5)	12.0370(7)	12.2514(8)	13.6367(12)	13.5794(4)	16.8069(18)
c/Å	19.9530(7)	19.9590(12)	19.4796(13)	18.0729(16)	17.9814(6)	20.971(2)
α/°	77.597(2)	77.711(2)	78.256(2)	109.112(2)	108.7492(12)	
β/°	88.046(2)	88.033(2)	86.361(2)	105.071(3)	105.7623(12)	93.166(4)
γ/°	72.215(2)	72.212(2)	74.106(2)	107.185(3)	106.8220(12)	
V/Å^3	2568.1(2)	2557.0(3)	2591.3(3)	2415.9(6)	2385.9(2)	5144.0(1)
Z	2	2	2	1	1	2
δ_{calcd}/g cm^{-3}	1.304	1.310	1.318	1.281	1.296	1.251
μ/mm^{-1}	0.937	0.985	0.854	0.990	1.049	0.856
Crystal size/mm	0.17 × 0.15 × 0.12	0.46 × 0.31 × 0.26	0.15 × 0.08 × 0.01	0.20 × 0.13 × 0.02	0.59 × 0.47 × 0.35	0.34 × 0.08 × 0.05
θ_{max}/°	27.52	27.53	27.57	26.73	27.59	27.50
Reflns. collected	54 053	28 596	56 676	25 041	35 739	56 537
Indep. reflns (Rint)	11 748 (0.0694)	11 719 (0.0316)	11 916 (0.1207)	9958 (0.1106)	10 801 (0.0271)	11 787 (0.2779)
Data/restraints/ parameters	11 748/2/565	11 719/9/587	11 916/12/614	99 58/12/542	10 801/6/533	11 787/12/568
Goof on F^2	1.044	1.045	0.991	0.943	1.048	0.958
R_1, wR_2 ($I > 2\sigma(I)$)	0.0455	0.0354	0.0518	0.0629	0.0371	0.0584
	0.1016	0.0889	0.0976	0.1206	0.0933	0.1104
R_1, wR_2 (all data)	0.0854	0.0534	0.1085	0.1514	0.0531	0.2469
	0.1209	0.1007	0.1217	0.1555	0.1036	0.1740
Largest diff. peak and hole/e Å^{-3}	0.591/–0.328	0.436/–0.330	0.446/–0.452	0.696/–0.420	0.657/–0.421	0.478/–0.498

metal ion is occupied by an aqua ligand. For first row transition metals, to the best of our knowledge, the only reported example with only five μ_2 carboxylate bridges in a $[M_3O(O_2CR)_5]$ core is an $Fe^{III}{}_2Fe^{II}$ acetate.[19] Selected bond lengths and bond angles are listed in Table 2. In all complexes the M^{II} site is clearly recognized from the metric of the $Fe^{III}{}_2M^{II}O$ moiety, as it possesses the longest M-μ_3O bond length. The relevant M-μ_3O bond lengths are in agreement with other reported $Fe^{III}{}_2M^{II}O$ cores[20-22] with the Fe–O bond distances as the smaller ones. In the case of complexes **2** and **3**, with Ni(II) and Mn(II) respectively, Fe-μ_3O bond lengths are quite similar with values, 1.8317(14) and 1.8433(14) Å (**2**) and 1.836(2) and 1.846(2) Å (**3**). For complex **1**, with Co(II), the Fe-μ_3O distances are more asymmetric with values 1.8827(19) and 1.8416(19) Å. The longest Fe–O bond distance agrees with the observed ones in the few crystallographically characterized reported examples of basic carboxylates with the [$Fe^{III}{}_2Co^{II}$-μ_3O] core.[20,21,23] Thus, the smallest Fe–O distance appears as an exception in these type of complexes. Regarding the M^{II}-μ_3O bond length values of 1.9958(19), 2.0230(14) and 2.119(2) Å for M = Co, Ni and Mn, all appear exceptionally large for these type of heteronuclear systems, except the one for Co, when comparing with the reported examples.[20,21,23] Overall, metal–metal distances within the triangle range between 3.186 and 3.368 Å, with complex **3** closely resembling an equilateral arrangement while complexes **1** and **2** are far away. With respect to the bidentate ligand, 2,2′-bipyridine, in the case of complexes **1** and **2** and 1,10-phenantroline in the case of complex **3**, the found M–N distances are within the usual range observed in related complexes involving these metal ions, Co^{II} and Ni^{II} for bpy[24] and Fe^{III} for phen.[25] As already mentioned in the discussion of the synthetic procedures, it is noticeable that in complex **3**, the phen ligand is not coordinating the divalent metal site, Mn^{II}, but the Fe^{III} site. The set of the five μ_2-pivalates shows distances that agree with the usually observed for this type of complexes, thus the whole structure pretty much resembles the complete $[M_3O(O_2CR)_6]$ basic carboxylate motif.[15] The remaining aqua and κ^2-pivalate ligands that complete the entire six coordinated metals environment exhibit typical M–O bond lengths for these ion–ligand combinations.

These heteronuclear basic carboxylate cores incorporating a bidentate ligand constitute a new archetype within this extensively studied family of first row transition metal clusters.

For complexes **4–6** the crystal structures reveal a supramolecular arrangement of covalently κ^4-μ-bipyrimidine bridged $Fe^{III}{}_2M^{II}O$ basic carboxylate cores, where each $Fe^{III}{}_2M^{II}O$ unit roughly corresponds to complexes **1–3** cores (Fig. 2). Compounds **4** and **5** are isostructural and crystallize in a triclinic cell, space group $P\bar{1}$, with one complex molecule and two acetonitrile solvent molecules in the unit cell; while compound **6** shows a $P21/n$ space group in a monoclinic cell, containing two complex molecules and eight acetonitrile solvent molecules. As observed for the structure packing in complexes **1–3**, the hexanuclear [$Fe^{III}{}_2M^{II}O$-μ–(bpym)$Fe^{III}{}_2M^{II}O$] clusters interact between them through H-bonds involving the apical aqua ligands. Because of the presence of aqua ligands in the axial positions at both sides of these hexanuclear clusters, the H-bonding interaction propagates affording a 1D network due to the bulky *tert*-butyl groups with the 1D chains well isolated (more than 12 Å closest M–M distance, see ESI†). In the case of complex **6**, the H-interaction motif exactly matches the one observed for complexes **1–3**, involving the aqua ligands and the neighbour molecule O-pivalate atoms. A different

Table 2 Selected bond lengths (Å) and M–μ_3-O–M angles (°) for **1–3**

1		**2**		**3**	
Fe1–O1	1.8827(19)	Fe1–O1	1.8317(14)	Fe2–O1	1.836(2)
Fe1–O6	2.0281(19)	Fe1–O3	2.0040(14)	Fe2–O11	1.986(2)
Fe1–O5	2.051(2)	Fe1–O9	2.0468(15)	Fe2–O4	2.025(2)
Fe1–O9	2.081(2)	Fe1–O7	2.0622(14)	Fe2–O3	2.031(2)
Fe1–O10	2.0955(18)	Fe1–O2	2.0823(14)	Fe2–N1	2.202(3)
Fe1–O12	2.148(2)	Fe1–O10	2.1575(15)	Fe2–N2	2.220(3)
Fe2–O1	1.8416(19)	Fe2–O1	1.8433(14)	Fe1–O1	1.842(2)
Fe2–O4	2.006(2)	Fe2–O5	1.9883(15)	Fe1–O14	1.984(2)
Fe2–O14	2.010(2)	Fe2–O11	2.0115(15)	Fe1–O8	2.006(2)
Fe2–O11	2.027(2)	Fe2–O6	2.0387(15)	Fe1–O5	2.046(2)
Fe2–O3	2.057(2)	Fe2–O12	2.0494(15)	Fe1–O6	2.078(2)
Fe2–O2	2.222(2)	Fe2–O8	2.2240(15)	Fe1–O7	2.231(2)
Co1–O1	1.9958(19)	Ni1–O1	2.0230(14)	Mn1–O1	2.119(2)
Co1–O7	2.048(2)	Ni1–O4	2.0250(15)	Mn1–O13	2.143(2)
Co1–O13	2.064(2)	Ni1–O14	2.0603(15)	Mn1–O10	2.151(2)
Co1–O8	2.081(2)	Ni1–O13	2.0660(16)	Mn1–O12	2.172(3)
Co1–N2	2.139(2)	Ni1–N1	2.0768(18)	Mn1–O2	2.214(2)
Co1–N1	2.142(2)	Ni1–N2	2.0771(18)	Mn1–O9	2.221(2)
Fe1 ··· Fe2	3.210	Fe1 ··· Fe2	3.186	Fe1 ··· Fe2	3.323
Fe1 ··· Co1	3.307	Fe1 ··· Ni1	3.284	Fe2 ··· Mn1	3.327
Fe2 ··· Co1	3.359	Fe2 ··· Ni1	3.368	Fe1 ··· Mn1	3.330
Fe1–O1–Co1	116.95(9)	Fe1–O1–Ni1	116.74(7)	Fe1–O1–Mn1	114.28(11)
Fe1–O1–Fe2	119.05(10)	Fe1–O1–Fe2	120.22(7)	Fe2–O1–Mn1	114.35(11)
Fe2–O1–Co1	122.15(10)	Fe2–O1–Ni1	121.11(7)	Fe1–O1–Fe2	129.26(12)

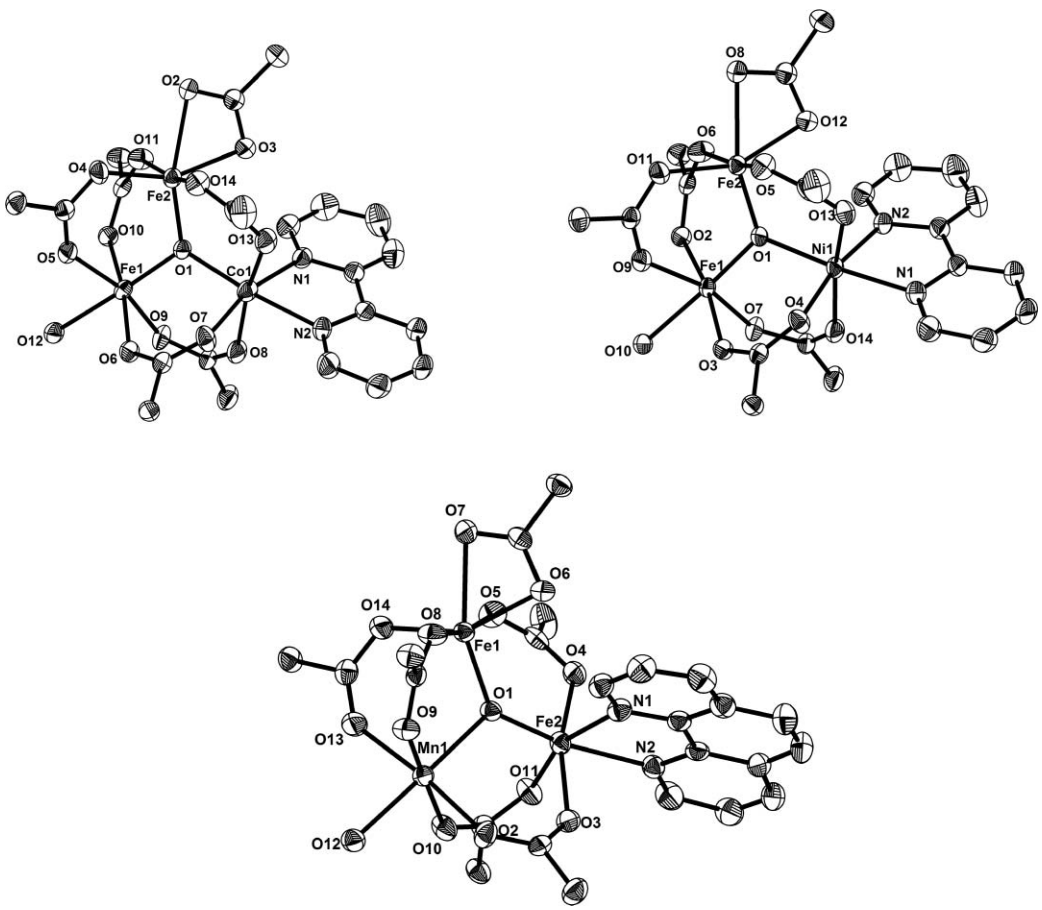

Fig. 1 ORTEP representation (ellipsoids at 30% probability) of complexes **1** (top left), **2** (top right) and **3** (bottom) molecular structures. *Tert*-butyl groups and H atoms were removed for sake of clarity. Only selected atoms were labeled.

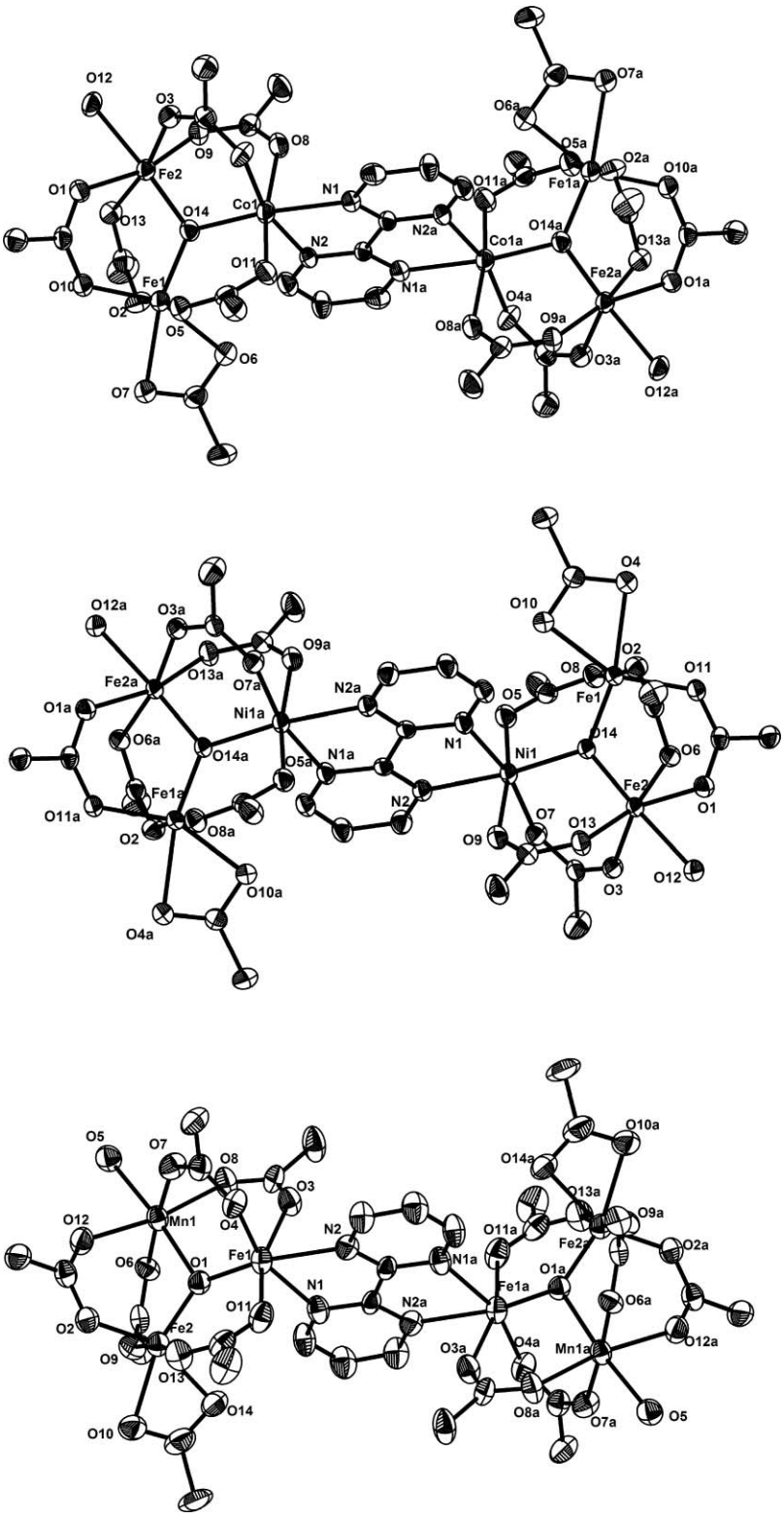

Fig. 2 ORTEP representation (ellipsoids at 30% probability) of complexes **4** (top), **5** (middle) and **6** (bottom) molecular structures. *Tert*-butyl groups and H atoms were removed for sake of clarity. Only selected atoms were labeled. Symmetry operation for the "a" labelled atoms: $-x, -y, -z$.

Table 3 Selected bond lengths (Å) and M–μ_3-O–M angles (°) for **4–6**

4		**5**		**6**	
Fe1–O14	1.837(3)	Fe1–O14	1.8382(17)	O1–Fe1	1.861(4)
Fe1–O10	1.972(4)	Fe1–O11	1.9707(17)	O4–Fe1	1.997(4)
Fe1–O5	2.008(4)	Fe1–O8	2.0024(18)	O11–Fe1	2.024(4)
Fe1–O2	2.074(4)	Fe1–O2	2.0824(17)	O3–Fe1	2.057(4)
Fe1–O6	2.086(4)	Fe1–O10	2.0884(18)	N1–Fe1	2.249(5)
Fe1–O7	2.177(4)	Fe1–O4	2.1770(18)	N2–Fe1	2.280(5)
Fe2–O14	1.843(3)	Fe2–O14	1.8389(17)	O1–Fe2	1.856(4)
Fe2–O3	2.007(4)	Fe2–O3	2.0098(17)	O2–Fe2	1.976(4)
Fe2–O9	2.018(4)	Fe2–O13	2.0168(18)	O9–Fe2	2.010(4)
Fe2–O1	2.052(4)	Fe2–O1	2.0504(17)	O13–Fe2	2.026(4)
Fe2–O13	2.063(3)	Fe2–O6	2.0701(16)	O14–Fe2	2.095(4)
Fe2–O12	2.127(4)	Fe2–O12	2.1292(19)	O10–Fe2	2.160(4)
Co1–O14	1.999(3)	Ni1–O14	1.9838(15)	O1–Mn1	2.086(4)
Co1–O11	2.053(4)	Ni1–O7	2.0249(18)	O12–Mn1	2.108(4)
Co1–O4	2.060(4)	Ni1–O5	2.0480(18)	O7–Mn1	2.138(4)
Co1–O8	2.086(4)	Ni1–O9	2.0504(19)	O8–Mn1	2.155(4)
Co1–N1	2.130(4)	Ni1–N2	2.091(2)	O5–Mn1	2.161(4)
Co1–N2	2.188(4)	Ni1–N1	2.142(2)	O6–Mn1	2.204(4)
Fe1 ⋯ Fe2	3.212	Fe1 ⋯ Fe2	3.203	Fe1 ⋯ Mn1	3.284
Fe2 ⋯ Co1	3.257	Fe2 ⋯ Ni1	3.240	Fe2 ⋯ Mn1	3.320
Fe1 ⋯ Co1	3.340	Fe1 ⋯ Ni1	3.333	Fe1 ⋯ Fe2	3.352
Co1 ⋯ Co1a[a]	5.764	Ni1 ⋯ Ni1a[a]	5.646	Fe1 ⋯ Fe1a[a]	6.007
Fe2–O14–Co1	115.86(17)	Fe2–O14–Ni1	115.84(8)	Fe1–O1–Mn1	112.49(19)
Fe1–O14–Co1	120.98(18)	Fe1–O14–Fe2	121.19(8)	Fe2–O1–Mn1	114.64(18)
Fe1–O14–Fe2	121.59(19)	Fe1–O14–Ni1	121.34(9)	Fe1–O1–Fe2	128.8(2)

[a] Symmetry operation, a: $-x$, $-y$, $-z$.

pattern is observed for complexes **4** and **5**, where one of the O-pivalate is replaced by a solvent acetonitrile molecule. The closest M–M distance of H-interacting moieties is longer than 5 Å in the three complexes. Noticeably, the metric of the molecular structure of these hexanuclear compounds closely agree with the observed for the related complexes **1–3** (Table 3). Pair-wise overlaying of related structures **1–4**, **2–5** and **3–6** leads to root mean square (rms) values for the atom to atom distance differences of 0.205, 0.203 and 0.201 Å, respectively (see ESI†). The latter have been calculated for all atoms (including the whole bridging L ligand) except for the methyl carbons of pivalate groups. In the three complexes both bpym bridged μ_3-oxo trinuclear fragments are related by an inversion center, hence, their molecular structures roughly correspond to bipyrimidine bridged complexes **1–3**. Regarding structural features of the M–bpym–M bridge, the observed M–N bond distances are comparable with the ones observed in related systems.[26-30] Surprisingly, complex **6** is only the second reported example of bpym bridged Fe(III) ions after the first example reported a decade ago.[30] In all cases the Fe_2M-μ_3O plane appears close to an orthogonal arrangement with respect to the plane of the bpym bridge which roughly contains the μ_3-O ligands. The N–M–O–M torsion angles are *ca.* 75° for complexes **4** and **5** and *ca.* 85° for complex **3**. In all cases the apical aqua ligands in both trinuclear cores point to opposite faces of the bridging bpym plane. Metal–metal distances mediated by the bpym ligand are 5.764, 5.646 and 6.007 Å in complexes **4–6** respectively, not so far away from the M ⋯ M inter-molecular distances mediated by H-bonding.

To our knowledge these complexes are the first example of a structurally characterized dimeric supramolecular arrangement of covalently bridged basic carboxylate cores prepared in a rational approach. Moreover, we are also reporting the basic carboxylate units included in the supramolecular dimeric structure showing strongly related geometric parameters.

Table 4 Mössbauer data fitting parameters of complexes **4–6**

Complex	Site	δ/mms^{-1}	ΔE_Q/mms^{-1}	$\Gamma/2$ [mms^{-1}]	Area [%]
4	I	0.63	0.93	0.18	50
	II	0.43	0.86	0.17	50
5	I	0.62	0.86	0.15	50
	II	0.45	0.78	0.15	50
6	I	0.64	0.90	0.16	50
	II	0.40	0.86	0.18	50

Mössbauer spectroscopy

Taking advantage of the iron content of these systems we performed preliminary Fe^{57}-Mössbauer studies for complexes **4–6** at 80 K (Fig. 3) to test for possible electronic isomerization after the assembly of the heteronuclear $Fe^{III}{}_2M^{II}$ cores. Confirming the crystallographic data, no signals corresponding to a possible high-spin Fe^{II} ion are observed, clearly excluding this possibility. Data can be successfully fitted with a 1 : 1 two site model involving two quadrupole-split doublets with typical parameters for six-coordinated high-spin Fe(III) in these type of complexes[15,31] (Fig. 3 and Table 4). It is therefore clear that the configuration $Fe^{III}{}_2M^{II}$ is retained in the three compounds **4–6**. Superposition of the spectra (see ESI†) and the narrow range observed in the isomer shift and the quadrupole splitting, 0.40–0.64 and 0.78–0.93 mms^{-1}, respectively confirms the similar local environments around the Fe ions. The two distinct Fe^{III} sites are in agreement with the crystallographic imposed inversion center that makes both $Fe^{III}{}_2M^{II}$ cores chemically equivalent.

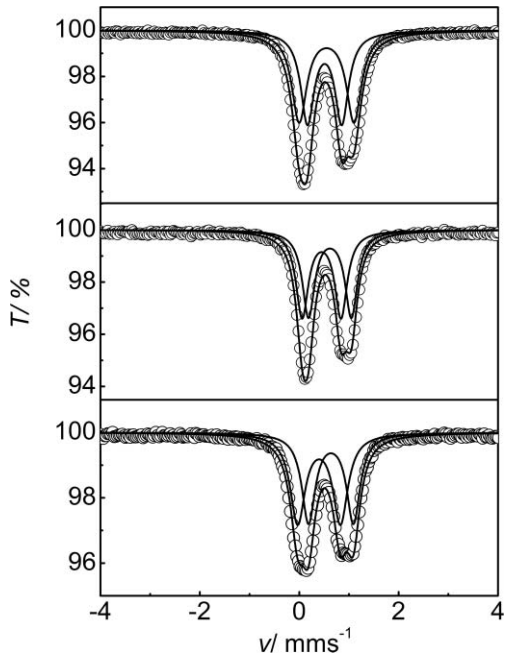

Fig. 3 Fe^{57} Mössbauer spectra at 80 K of complexes **4–6** (top to bottom). Open circles: experimental data; full line: fitting with parameters of Table 4.

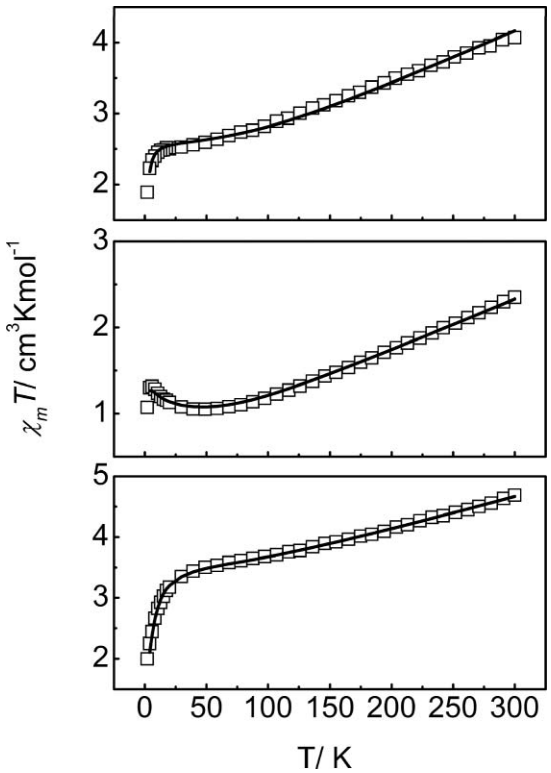

Fig. 4 Open squares: $\chi_m T$ *vs.* T plots at 1 T of complexes **1–3** (top to bottom); full line: best fitting with Hamiltonian of eqn (2) (see text).

Magnetic properties

Single basic carboxylates $Fe^{III}_2M^{II}LL$ (1–3). DC magnetic susceptibility of complexes **1–3** was measured in the temperature range 2–300 K (Fig. 4) under an applied field of 1 T. In all cases, competing antiferromagnetic exchange interactions are expected as has been previously observed for these μ_3-oxo triangular systems.[15] This is confirmed by the experimental $\chi_m T$ data. At 300 K $\chi_m T$ values of 4.04 (**1**), 4.34 (**2**) and 4.69 (**3**) cm^3 K mol^{-1} are observed, all well below the expected values for two isolated high-spin Fe(III) ions and the corresponding high-spin M^{II} ion, 10.62, 9.75 and 13.12 cm^3 K mol^{-1} with $g_{av} = 2$, respectively. With decreasing temperature the $\chi_m T$ product smoothly decrease down to 50 K where an abrupt drop in case of complexes **1** and **3** down to 1.89 and 1.99 cm^3 K mol^{-1}, respectively, at 2 K is observed, which may be attributed to inter-molecular interactions being operative. For complex **2** an increase to 3.24 cm^3 K mol^{-1} at 6 K and then a drop to 2.93 cm^3 K mol^{-1} at 2 K is found. The non-zero $\chi_m T$ values at 2 K suggest the presence of magnetic ground states for these triangular systems.

We attempted a full fitting of the data by obtaining the energy of the different spin states and calculating the molar susceptibility with eqn (1) for all possible field orientations:

$$\chi = \frac{1}{H}\frac{N\sum_n \left(-\partial E_i/\partial H\right)\exp\left(-E_i/kT\right)}{\sum_i \exp(-E_i/kT)} \quad (1)$$

The energy of the different spin levels is obtained through diagonalization of the suitable Hamiltonian. In this case, the Heisenberg spin Hamiltonian (with the corresponding Zeeman terms) describing the isotropic exchange interactions within the Fe_2M triangle (Scheme 2) is given by eqn (2), where J_1 refers to the interactions between Fe1 ⋯ M and Fe2 ⋯ M and J_2 refers to the Fe1 ⋯ Fe2 interaction:

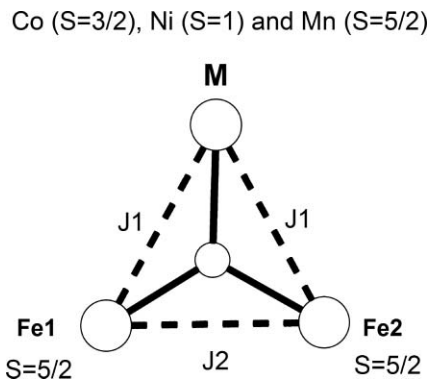

Scheme 2 Exchange coupling pattern in triangular complexes **1–3**.

$$\hat{H} = -2J_1(\hat{S}_{Fe1}\bullet\hat{S}_M + \hat{S}_{Fe2}\bullet\hat{S}_M) - 2J_2(\hat{S}_{Fe1}\bullet\hat{S}_{Fe2}) \quad (2)$$

Rigorously, a 3J model should be employed as both Fe sites are not chemically identical but a 2J model is retained to avoid over-parameterization. The energies of the resultant total spin states S_T, which are eigenfunctions of the Hamiltonian in this coupling scheme, are given by eqn (3), where $\hat{S}_A = \hat{S}_{Fe1} + \hat{S}_{Fe2}$. The overall multiplicities of the spin system are 144, 108 and 216, made up of 20, 16 and 27 individual spin states ranging from $S_T = 1/2$ to 13/2, 0 to 6 and 1/2 to 15/2 for **1**, **2** and **3** respectively.

$$E\,|\,S_T,S_A\rangle = -J_1[S_T(S_T+1) - S_A(S_A+1)] - J_2[S_A(S_A+1)] \quad (3)$$

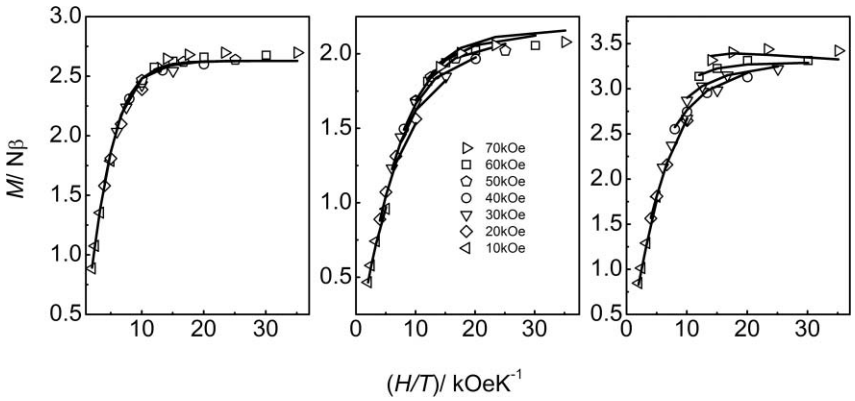

Fig. 5 Plot of reduced magnetization ($M/N\beta$) *vs.* H/T for complexes **1–3** (left to right) in the 2–5 K range. The solid lines are the best fitting of the data (see text).

Satisfactory fitting of the experimental data in the whole temperature range (with exception of the very low T range, below 4 K) were obtained (Fig. 4) with the following parameters: $g_{av} = 2.76 \pm 0.01$, $J_1 = -34 \pm 1$ cm^{-1} and $J_2 = -85 \pm 2$ cm^{-1} ($R = 3.39 \times 10^{-4}$); $g_{av} = 2.28 \pm 0.03$, $J_1 = -34 \pm 2$ cm^{-1} and $J_2 = -74 \pm 2$ cm^{-1} ($R = 3.59 \times 10^{-4}$); $g_{av} = 2.07 \pm 0.01$, $J_1 = -20.2 \pm 0.6$ cm^{-1} and $J_2 = -66 \pm 2$ cm^{-1} ($R = 2.18 \times 10^{-4}$) for **1**, **2** and **3** respectively. These values for the exchange coupling constants J_{Fe-Fe} and J_{Fe-M} are in close agreement with the ones found previously in related heteronuclear basic carboxylates compounds.[15,20,32] In these type of triangular systems the ratio between both coupling constants J_1/J_2 determines the identity of the ground state spin multiplet, S_T. From the above quoted exchange coupling constant values, the following J_1/J_2 ratios are obtained: 0.40, 0.46 and 0.31 which afford the following spin ground states (according to eqn (3)) a degenerate $S = 1/2$ ($|1/2,1\rangle$); $S=3/2$ ($|3/2,0\rangle$) pair, $S = 1$ ($|1,0\rangle$) and $S=3/2$ ($|3/2,1\rangle$), respectively. A close in energy low lying first excited state is predicted for complexes **2** and **3**, being an $S = 0$ (at 12 cm^{-1}) and an $S = 5/2$ (at 8 cm^{-1}) respectively.

In order to obtain more information about the spin ground states of these triangular compounds, we performed magnetization measurements in the range 2–5 K under magnetic external fields up to 70 kOe (Fig. 5). In the three complexes saturation of the magnetization is reached, but only in complex **1** the isofield lines completely superimpose. Saturation values found are 2.08, 3.42 and 2.70 $N\beta$ for **1**, **2** and **3** respectively. Only for complex **2** a satisfactory data fitting assuming an isolated ground state, in this case $S = 1$, can be obtained. A negative zero-field splitting D parameter must be added, by employing Hamiltonian of eqn (4):

$$\hat{H} = g\beta\hat{S}H + D(\hat{S}^2 - S(S+1)/3) \quad (4)$$

The obtained fitting parameters for the $S = 1$ ground state are: $g = 2.24 \pm 0.03$, $D = -5 \pm 1$ cm^{-1} ($R = 4.19 \times 10^{-4}$). Whereas the g value nicely agrees with susceptibility data, the D value cannot be reliably extracted from there but it appears clearer in the reduced magnetization data. No possible fitting is obtained when considering a positive value of D. This rather big value of D is within the usual range observed for Ni(II) ion[33] agreeing with the composition of this $S = 1$ ground state: ($|1,0\rangle$) which has no Fe(III) component.

In the case of complex **3**, it is necessary to include in the model the first excited state with $S = 5/2$ (from susceptibility data) in addition to the $S = 3/2$ ground state, to properly fit the experimental data. When the energy of the quintuplet is fit, together with a unique g value for both multiplets, the following best fitting parameters are obtained: $g = 2.19 \pm 0.01$ and $E(S=5/2) = 12.6 \pm 0.5$ cm^{-1} ($R = 3.11 \times 10^{-4}$). This energy value obtained for the excited quintuplet is in close agreement with the susceptibility data.

The case of complex **1** is the most striking. From susceptibility data an almost degenerate ground state with $S = 1/2$ and $S = 3/2$ is predicted. However, no possible data fitting can be performed under this assumption, even if some energy difference between both multiplets is taken into consideration. On the other hand, the data is reasonably fit with the assumption of an $S = 1/2$ ground state with a large g value, $g = 5.26 \pm 0.02$ ($R = 1.83 \times 10^{-4}$). A well isolated ground state with angular moment $J = 1/2$ and a large g value has been also shown for a quite similar triangular $Fe^{III}_2Co^{II}$ basic carboxylate.[32] This ground state is calculated considering an additional spin-orbit contribution arising from the angular moment $L = 1$ coupled to the Co^{II} ion $S = 3/2$ that adds to the HDvV Hamiltonian of eqn (2), suitable for the high-spin d^7 Co^{II} configuration. Even if this model has a high over-parametrization risk, there is no possibility of fitting our data with reasonable parameters values. At the same time the J_1 and J_2 values found in the Fe^{III}_2Co complex – mathematically treated by Tsukerblat *et al.* with this model that includes the orbital angular contribution – are almost identical to the ones we found for complex **1** using HDvV Hamiltonian of eqn (2).[32] It could be possible that the isotropic restriction imposed in this model is no longer valid in the case of complex **1**, as the bpy ligand considerably breaks the octahedral symmetry. Any attempt to fit the low temperature data (below 20 K) under the assumption of a unique populated Kramer doublet for Co^{II} was also unsuccessful, as unreliable values for the Fe–Fe exchange coupling constant were obtained. Even if a convincing precise model cannot be employed, magnetization data at least, strongly suggest a well isolated ground state with a half-integer angular moment.

In summary, magnetic data show non-zero spin ground states for the triangular $Fe^{III}_2M^{II}$ cores which are the building blocks for the supramolecular dimeric hexanuclear clusters **4–6**.

$\{Fe^{III}_2M^{II}O\}_2$(μ-bpym) complexes (4–6). As for the trinuclear complexes, DC magnetic susceptibilities were measured in the

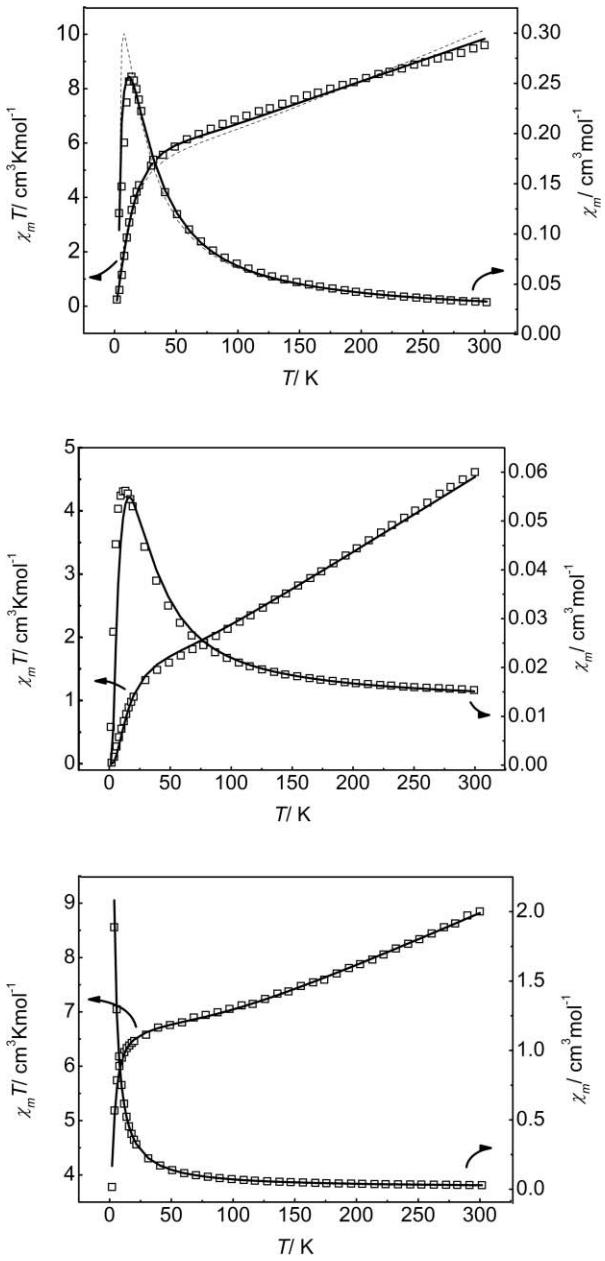

Fig. 6 Open squares: $\chi_m T$ *vs.* T plots at 1 T of complexes **4–6** (top to bottom); full line: best fitting with Hamiltonian of eqn (5) and 6 (see text). For complex **4**, full line: best fitting with fixed $g_{av} = 2.76$ and free J coupling constants; dashed line: best fitting with fixed J_1 and J_2 and free g_{av} (see text).

temperature range 2–300 K (Fig. 6) under an applied field of 1 T for complexes **4–6**. A weak antiferromagnetic coupling is expected to operate between the bipyrimidine bridged trinuclear cores, as all previously reported examples of interacting metallic sites through this ligand show this type of magnetic interaction, which is usually in the order of a few wavenumbers.[12,26-28 30,34,35] In fact, this is clearly observed at low temperature as a maximum in the χ_m *vs.* T plot (absent in the isolated trinuclear partner compounds) for complexes **4** and **5**, at 12 and 14 K respectively. In the case of complex **6**, no distinctly differences to the susceptibility data of complex **3** are observed. When looking at the high temperature range a rough concordance in the $\chi_m T$ *vs.* T plot is found, between complexes **4–6** data and complexes **1–3** data after accounting for the presence of two Fe_2MO units and normalizing the small differences in g_{av} value (see overlayed plots in the ESI†). Thus, as a consequence of the antiferromagnetic coupling between Fe_2MO units through the bpym bridge, only at low temperature the plots deviate (with exception of complex **6**). This apparent decoupled behaviour between the intra-Fe_2MO μ_3-oxo mediated magnetic exchange interactions and the inter-Fe_2MO μ-bpym mediated magnetic exchange interaction, is explained by the relative magnitude of the J constant coupling strengths. The intra μ_3-oxo core interactions being much larger than the inter μ-bpym one. Based on this observation, we attempted to fit the experimental data restraining the J values that describe the intra-Fe_2MO μ_3-oxo interactions to the values obtained from complexes **1–3** $\chi_m T$ *vs.* T data fittings, such to avoid over-parameterization. The spin Hamiltonian we employed to describe the magnetic behaviour in complexes **4–6** are the ones in eqn (5) and eqn (6) for complexes **4–5** and **6**, respectively (see Scheme 3):

$$\hat{H} = -2J_1(\hat{S}_{Fe1} \bullet \hat{S}_{M1} + \hat{S}_{Fe2} \bullet \hat{S}_{M1} + \hat{S}_{Fe3} \bullet \hat{S}_{M2} + \hat{S}_{Fe4} \bullet \hat{S}_{M2}) - 2J_2(\hat{S}_{Fe1} \bullet \hat{S}_{Fe2} + \hat{S}_{Fe3} \bullet \hat{S}_{Fe4}) - 2J_3(\hat{S}_{M1} \bullet \hat{S}_{M2}) \quad (5)$$

$$\hat{H} = -2J_1(\hat{S}_{Fe1} \bullet \hat{S}_{Mn1} + \hat{S}_{Fe2} \bullet \hat{S}_{Mn1} + \hat{S}_{Fe3} \bullet \hat{S}_{Mn2} + \hat{S}_{Fe4} \bullet \hat{S}_{Mn2}) - 2J_2(\hat{S}_{Fe1} \bullet \hat{S}_{Fe2} + \hat{S}_{Fe3} \bullet \hat{S}_{Fe4}) - 2J_3(\hat{S}_{Fe2} \bullet \hat{S}_{Fe3}) \quad (6)$$

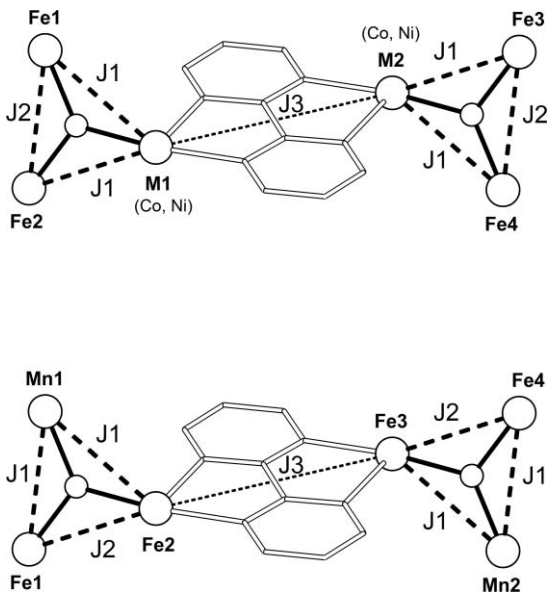

Scheme 3 Exchange coupling pattern in complexes **4** and **5** (top) and **6** (bottom).

Fitting of the experimental data employing the MAGPACK package[36] (with J_1 and J_2 fixed according to compounds **1–3** obtained values, Fig. 6) afforded the following parameters: $g_{av} = 3.07 \pm 0.03$, J_1 (fixed) $= -34$ cm^{-1}, J_2 (fixed) $= -85$ cm^{-1}, $J_3 = -2.4 \pm 0.3$ ($R = 1.2 \times 10^{-3}$); $g_{av} = 2.26 \pm 0.01$, J_1 (fixed) $= -34$ cm^{-1}, J_2 (fixed) $= -74$ cm^{-1}, $J_3 = -6.6 \pm 0.3$ ($R = 5.6 \times 10^{-4}$) and $g_{av} = 2.01 \pm 0.01$, J_1 (fixed) $= -20.2$ cm^{-1}, J_2 (fixed) $= -69$ cm^{-1}, J_3 (fixed) $=0$ ($R = 2.7 \times 10^{-4}$) for **4**, **5** and **6**, respectively. For complex **6**, there is no way to determine a definite value for J_3, as no fitting improvement is achieved when including this coupling constant in

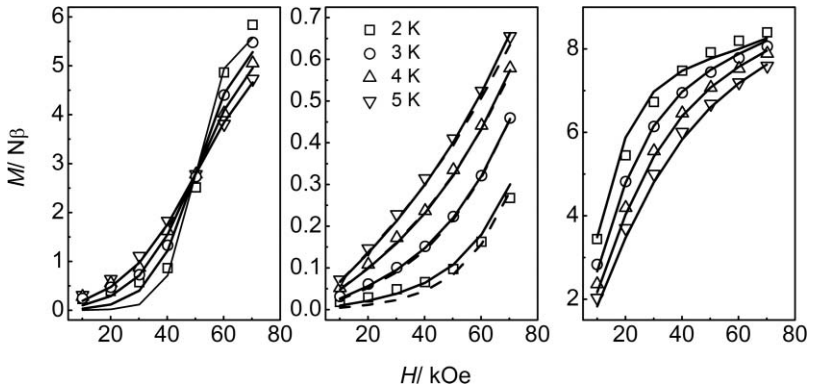

Fig. 7 Plot of reduced magnetization ($M/N\beta$) *vs.* H for complexes **4–6** (left to right) in the 2–5 K range. The solid lines are the best fitting of the data (see text). For complex **5**, full line: best fitting with fixed $D = -5$ cm^{-1}; dashed line: best fitting without zfs term (see text).

the model. Hence, it was fixed to the value of zero and only the g_{av} fitting parameter was left free. Regarding complex **4** a much better factor agreement is obtained when a more realistic g_{av} value is used. When g_{av} is fixed according to the data fitting results in complex **1**, and all three J coupling constants are fit, an improved agreement factor, $R = 5.6 \times 10^{-4}$ is obtained with the following best fitting parameters: g_{av} (fixed) = 2.76, $J_1 = -13 \pm 2$ cm^{-1}, $J_2 = -85 \pm 8$ cm^{-1} and $J_3 = -2.2 \pm 0.1$ cm^{-1} (Fig. 6, full line). While the J_3 value remains essentially the same, a smaller J_1 value is obtained. As the orbital angular contributions are not included, the susceptibility data fitting is probably hampered in complex **4**. However, it is certainly more correct kept this way as this avoids over-parametrization and consequently misleading results. The exchange interaction coupling constant J_3 values obtained for the μ-bpym pathway are in close agreement with the ones observed in other M–μ(bpym)–M systems, with M = Co(II) and Ni(II).[26,28,35] For M = Fe(III) in the only reported corresponding example [Fe^{III}_2(bpym)$Cl_6(H_2O)_2$],[30] a very weak antiferromagnetic J coupling parameter was found to be < 1 cm^{-1}. This confirms the difficulty we had to determine J_3 for complex **6**.

In order to get a deeper insight in the magnetic behaviour of the complexes, we performed magnetization measurements in the range 2–5 K under external magnetic fields up to 70 kOe, shown in Fig. 7 as variable field isotherms. With the exception of complex **6** data, that resemble the magnetization data obtained for the related Fe_2Mn trinuclear complex **3**, distinctive *M vs. H* data plots for complexes **4** and **5** were obtained. They are characteristic of a non-magnetic ground state with low lying magnetic excited states and subsequent energy level crossing. Their profiles constitute unequivocal evidence of antiferromagnetic exchange coupling through the bpym bridge.

Magnetic susceptibility data suggest that these complexes behave as isolated Fe_2MO cores with a weak interaction through the bpym bridge. In consequence, we first attempted to fit magnetization data as isolated identical spin ground sates ($S_1 = S_2$) (arising from intra-Fe_2MO core coupling) interacting through μ-bpym mediated J exchange parameter. The corresponding Hamiltonian is described in eqn (7):

$$\hat{H} = g\beta(\hat{S}_1 + \hat{S}_2)H - 2J(\hat{S}_1 \cdot \hat{S}_2) \quad (7)$$

In the case of complex **6**, no satisfactory fitting is possible, in agreement with the results obtained for complex **3**, where two close spaced lying levels were found instead of a well isolated spin ground state. On the other hand, satisfactory fitting were achieved in the case of complexes **4** and **5**. For complex **5**, relying on magnetic data results extracted for the related complex **2**, Fe_2Ni, the involved spins are $S_1 = S_2 = 1$, with best fitting parameters, $g = 1.96 \pm 0.05$ and $J = -4.4 \pm 0.1$ cm^{-1} ($R = 9.3 \times 10^{-4}$). If, as observed for complex **2**, a fixed ZFS parameter, D, is included (through addition of a Hamiltonian term like eqn (4)), the following best fitting parameters are obtained: $g = 2.09 \pm 0.06$, $J = -4.4 \pm 0.1$ cm^{-1} and D (fixed) = −5 cm^{-1} ($R = 9.1 \times 10^{-4}$). The relevant J parameter remains unchanged independently of the inclusion of the ZFS contribution and is in agreement with the J_3 value found in the susceptibility data. A similar result is obtained for complex **4**. As observed in the related complex **1**, data can be reasonably fitted as two interacting $S = 1/2$, with an unusual high g value. Best fitting parameters are: $g = 5.7 \pm 0.2$ and $J = -6.7 \pm 0.3$ cm^{-1} ($R = 2.7 \times 10^{-3}$). The observed level crossing at a field of about 50 kOe, is well reproduced with this model and any attempt of fitting with the complete Hamiltonian of eqn (5) completely failed. The J value is somewhat bigger than the J_3 value obtained from susceptibility data, but should be related to the fictitious $S = 1/2$ spin arising from the combined effect of spin–orbit coupling and the orbital momentum contribution.

Magnetization data of complex **6**, allows determining a non-zero value for J_3, whose assessment is not possible solely from susceptibility data. By using the Hamiltonian of eqn (6), with fixed values for J_1 and J_2, the following best fitting parameters are obtained: $g_{av} = 1.95 \pm 0.02$, J_1 (fixed) = −20.2 cm^{-1}, J_2 (fixed) = −69 cm^{-1}, $J_3 = -1.1 \pm 0.2$ ($R = 9.9 \times 10^{-4}$). If a rigorous value of zero for J_3 parameter (no interaction through the bpym bridge) is set, the high field profile of the magnetization isotherms cannot be properly reproduced.

It comes clear from the above results that the hexanuclear complexes behave as weakly interacting pairs of basic carboxylate sharing the Fe_2M-μ_3O motif. This interaction is mediated by the 2,2′-bipyrimidine ligand, already known to propagate antiferromagnetic interaction between first row transition metals. In the case of complexes **4** and **5**, the whole system behaves at low temperature as two isolated spin entities,

Table 5 DFT calculated exchange coupling constants J for complexes **1–6**

	J_{1a}/cm^{-1}	J_{1b}/cm^{-1}	J_2/cm^{-1}	J_3/cm^{-1}	
	Ruiz formalism (Ising formalism)				Experimental
1	−29.6 (−35.6)	−30.8 (−37.0)	−61.7 (−74.1)	—	$J_1 = -34 \pm 1$ cm^{-1} $J_2 = -85 \pm 2$ cm^{-1}
2	−31.7 (−38.1)	−39.2 (−47.1)	−68.4 (−82.1)	—	$J_1 = -34 \pm 2$ cm^{-1} $J_2 = -74 \pm 2$ cm^{-1}
3	−27.3 (−32.8)	−34.9 (−41.8)	−70.4 (−84.5)	—	$J_1 = -20.2 \pm 0.6$ cm^{-1} $J_2 = -66 \pm 2$ cm^{-1}
4	−29.6 (−35.6)	−31.6 (−37.9)	−66.9 (−80.3)	−2.1 (−2.7)	$J_1 = -34$ cm^{-1} (-13 ± 2 cm^{-1}) $J_2 = -85$ cm^{-1} (-85 ± 8 cm^{-1}) $J_3 = -2.4 \pm 0.3$ cm^{-1} (-2.2 ± 0.1 cm^{-1})
5	−34.1 (−40.9)	−36.7 (−44.1)	−67.0 (−80.4)	−5.8 (−8.8)	$J_1 = -34$ cm^{-1} $J_2 = -74$ cm^{-1} $J_3 = -6.6 \pm 0.3$ cm^{-1} (-4.4 ± 0.1 cm^{-1})
6	−32.0 (−38.4)	−54.4 (−65.2)	−69.3 (−83.2)	−1.3 (−1.4)	$J_1 = -20.2$ cm^{-1} $J_2 = -66$ cm^{-1} $J_3 = -1.1 \pm 0.2$ cm^{-1}

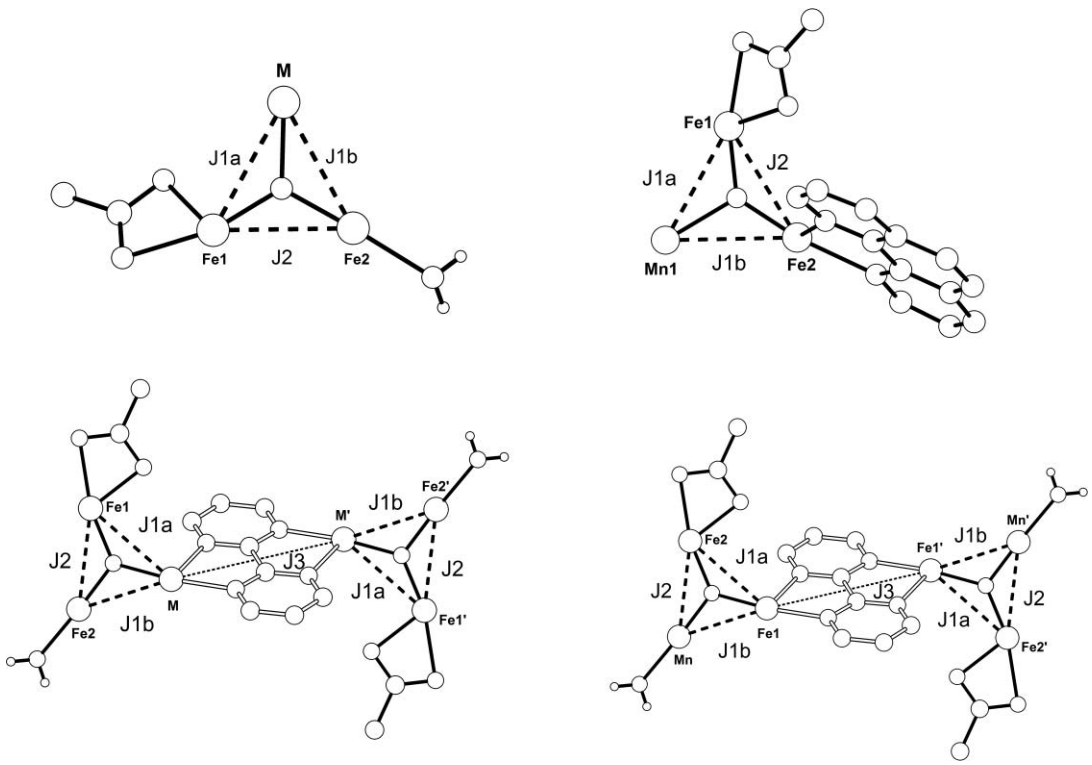

Scheme 4 DFT calculated exchange coupling constants pattern in complexes **1–3** (top) and **4–6** (bottom).

$S = 1/2$ and $S = 1$ respectively, covalently bridged and weakly interacting.

DFT calculations

To get a deeper understanding on the magnetic interactions present in these complexes, we performed broken-symmetry (BS) DFT calculations at the X-ray geometry for all of them. Calculated values for the different isotropic exchange coupling constants (Scheme 4) were obtained. We used the medium size basis set, LanL2DZ, which we previously successfully employed in related systems and provides a size/computing time ratio suitable for big clusters computations affording reliable computed values.[26,37] The results are shown in Table 5. When comparing with the values obtained from experimental data fitting, the accuracy is quite remarkable. In all cases the correct signs for the J values are predicted, supporting the expected and observed antiferromagnetic interaction within the Fe_2MO cores and between them. Calculated values support the equivalency between intra-Fe_2MO core exchange coupling constants in the isolated complexes **1–3** and the interacting **4–6** ones. The Ising formalism over-estimates the experimental J values in comparison with the more accurate results coming from the Ruiz method. The different J_{1a} and J_{1b} coupling constants afford a mean value in close agreement with the experimental J_1 value. Clearly, both theoretical calculated coupling constants cannot be independently extracted from the experimental data fitting due to

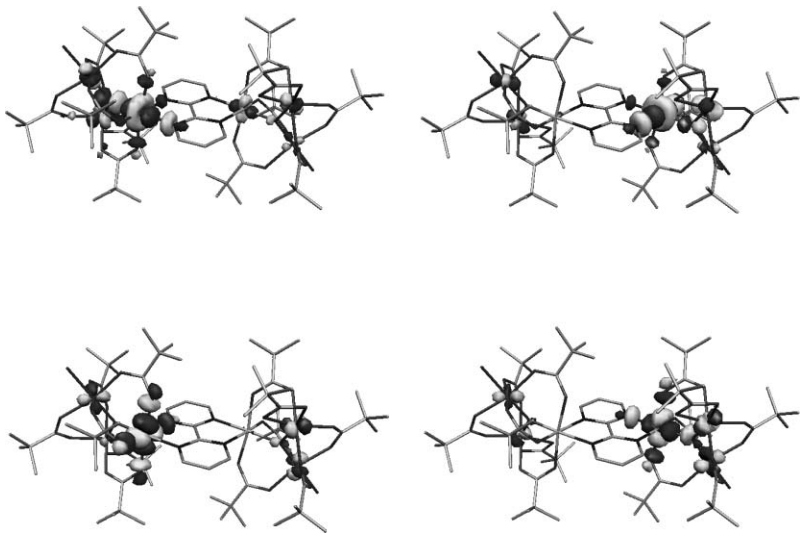

Fig. 8 Natural localized orbital pairs with unitary occupancy, centered at Ni(II) sites that show σ-type exchange pathway through the bipyrimidine bridge in complex **5**.

over-parameterization. In all cases, as expected, the bigger J value corresponds to J_2, which couples both Fe(III) sites through the shortest M–O–M pathway. The only notably discrepancy appears in the obtained values for complex **6**. In this case an over-estimated value for J_{1b}, when comparing with experimental results and even with the calculated value for complex **3**, arises from the calculation. Even if some metric differences can be found in the Fe_2MnO core between complexes **3** and **6**, they cannot easily explain this discrepancy.

Probably the most relevant information obtained from DFT calculations is the inter-Fe_2MO core exchange coupling, J_3, value. In complexes **4–6** the accordance with the experimental data is remarkable, affording antiferromagnetic exchange interactions as expected. Previous theoretical calculations show that the HOMO σ-type orbitals of the bipyrimidine bridge are responsible for the exchange pathways.[26,38] Inspection of the magnetic orbitals involved shows that these pathways are also observed in our systems (Fig. 8 and ESI†).

Conclusion

Following a rational approach we have successfully prepared a family of covalently linked basic carboxylate cores with $Fe^{III}{}_2M^{II}$ (M = Co, Ni and Mn) composition using 2,2′-bipyrimidine as a bridging ligand. Most important, we also succeeded in synthesizing the single building blocks. Their structures closely resemble the ones in the dimeric supramolecular compounds [$Fe^{III}{}_2M^{II}$-μ(bpym)–$Fe^{III}{}_2M^{II}$]. Thus we were able to study separately the magnetic properties of the isolated triangular moieties as well as the covalently linked ones. From susceptibility and magnetization data a weak antiferromagnetic interaction of the order of a few wavenumbers between the covalently linked heterometallic trinuclear units was found. DFT calculations supported these results. Depending on the identity of the metal M, different spin ground states are obtained for the isolated basic carboxylate building blocks. In the case of M^{II} being Ni^{II} and Co^{II} ground states well isolated from the first excited spin states are found. In summary, our rational approach opens a new way for engineering at the molecular level supramolecular systems based on third row transition metal clusters bearing isolated spin ground states. This is a key feature regarding what chemists can contribute within the field of quantum computing and spintronics.

Experimental

Material and physical measurements

The complexes $[Fe_3O((CH_3)_3COO)_6(H_2O)_3]ClO_4$,[39] $[Co_2(OH_2)((CH_3)_3COO)_4((CH_3)_3COOH)_4]$,[40] $[Ni_2(OH_2)((CH_3)_3COO)_4((CH_3)_3COOH)_4]$[41] and the ligand 2,2′-bipyrimidine[42] were prepared following previously reported procedures. Sodium trimethylacetate was prepared by reaction of trimethylacetic acid with sodium hydroxide in methanol. All other chemicals were reagent grade and used as receive without further purification. Elemental analysis for C, H and N were performed on a Foss Heraeus Vario EL elemental analyzer. Magnetic measurements were performed with a Quantum Design MPMS XL SQUID magnetometer. DC measurements were conducted from 2 to 300 K at 1 T and from 2 to 5 K under applied field up to 7 T. All measurements were performed on restrained polycrystalline samples in order to avoid field induced re-orientation of the microcrystals. Experimental magnetic data were corrected for the diamagnetism of the sample holders and of the constituent atoms (Pascal's tables). Mössbauer data were recorded on an alternating constant-acceleration spectrometer. The minimum experimental line width was 0.3 mms^{-1} (full width at half-height). The sample temperature was maintained constant in an Oxford Instruments. Isomer shifts are quoted relative to iron metal at 300 K.

Synthesis of the complexes

$[Fe^{III}{}_2M^{II}\mu_3\text{-}(O)\mu\text{-}((CH_3)_3COO)_5((CH_3)_3COO)(H_2O)(bpy)]\cdot 2H_2O$, M = Co (1), Ni (2). 0.1 g (0.1 mmol) of $[Fe_3O((CH_3)_3COO)_6(H_2O)_3]ClO_4$ was dissolved in 10 ml of acetonitrile affording a clear orange solution. To this solution

0.016 g (0.1 mmol) of solid 2,2′-bipyridine (bpy) was added under stirring. Once bpy had completely dissolved after a few minutes, a dark brown solution was obtained. To this solution, 0.05 g (0.05 mmol) of $[M_2(OH_2)((CH_3)_3COO)_4((CH_3)_3COOH)_4]$, M = Co(**1**), Ni(**2**) dissolved in minimum amount of acetonitrile was added immediately, affording a darker red-brown solution. It was filtered to remove some insoluble solid residue, and the clear final solution left undisturbed slowly evaporating at room temperature. After 3–4 days, dark red blocks suitable for X-ray diffraction measurements were obtained. After selecting one specimen for measurement, they were filtered, washed with a small amount of cold acetonitrile and vacuum dried (**1**: 0.012 g, 12%; **2**: 0.023 g, 23%). Elemental analysis calcd (%) for **1**, $C_{40}H_{68}CoFe_2N_2O_{15}$: C 48.65, H 6.94, N 2.84; found: C 48.31, H 7.05, N 2.55. **2**, calcd (%) C_{40} H_{68} Fe_2 N_2 Ni O_{15}: C 48.66, H 6.94, N 2.84; found: C 49.23, H 7.05, N 2.76.

$[Fe^{III}_2Mn^{II}\mu_3$-(O)μ-$((CH_3)_3COO)_5((CH_3)_3COO)(H_2O)(LL)]\cdot 2H_2O$, LL = phen (3). 0.1 g (0.1 mmol) of $[Fe_3O((CH_3)_3COO)_6(H_2O)_3]ClO_4$ was dissolved in 10 ml of acetonitrile affording a clear orange solution. To this solution 0.1 mmol of solid LL (0.02 g, phen, 0.016 g, bpy) was added under stirring. Once LL had completely dissolved after a few minutes, a dark brown solution was obtained. To this solution, 0.036 g (0.1 mmol) of solid $Mn(ClO_4)_2\cdot 6H_2O$ followed by 0.025 g of $Na((CH_3)_3COO)$ (0.2 mmol) were added with vigorous stirring. After 1 h of further stirring the mixture was filtered and the resulting solution left undisturbed slowly evaporating at room temperature. In a few days dark red blocks suitable for X-ray diffraction measurements were obtained. After selecting one specimen for measurement, they were filtered, washed with a small amount of cold acetonitrile and vacuum dried (0.016 g, 16%). Elemental analysis calcd (%) for **3**, $C_{42}H_{68}Fe_2MnN_2O_{15}$: C 50.06, H 6.80, N 2.78; found: C 50.12, H 6.73, N 2.48.

$[Fe^{III}_2M^{II}\mu_3$-(O)μ-$((CH_3)_3COO)_5((CH_3)_3COO)(H_2O)]_2$(μ-bpym)$\cdot x$ H_2O, M = Co (4) (x = 0), Ni (5) (x = 2.5). 0.1 g (0.1 mmol) of $[Fe_3O((CH_3)_3COO)_6(H_2O)_3]ClO_4$ was dissolved in 10 ml of acetonitrile affording a clear orange solution. To this solution 0.008 g (0.05 mmol) of solid 2,2′-bipyrimidine (bpym) was added under stirring. Once bpym had completely dissolved after a few minutes, a dark brown solution was obtained. To this solution, 0.05 g (0.05 mmol) of $[M_2(OH_2)((CH_3)_3COO)_4((CH_3)_3COOH)_4]$, M = Co(**4**), Ni(**5**) dissolved in minimum amount of acetonitrile was added immediately, affording a darker red-brownish solution. It was filtered to remove some insoluble solid residue, and the clear final solution left undisturbed slowly evaporating at room temperature. After 3–4 days, dark red blocks suitable for X-ray diffraction measurements were obtained. After selecting one specimen for measurement, they were filtered, washed with acetonitrile and vacuum dried (**4**: 0.064 g, 72%; **5**: 0.058 g, 63%). Elemental analysis calcd (%) for **4**, $C_{68}H_{118}Co_2Fe_4N_4O_{28}$: C 45.86, H 6.68, N 3.15; found: C 45.92, H 6.76, N 2.95. **5**, calcd $C_{68}H_{123}Fe_4N_4Ni_2O_{30.5}$: C 44.74, H 6.79, N 3.07; found: C 44.77, H 5.99, N 3.05.

$[Fe^{III}_2Mn^{II}\mu_3$-(O)μ-$((CH_3)_3COO)_5((CH_3)_3COO)(H_2O)]_2$(μ-bpym)$\cdot 2.5H_2O$ (6). 0.1 g (0.1 mmol) of $[Fe_3O((CH_3)_3COO)_6(H_2O)_3]ClO_4$ was dissolved in 10 ml of acetonitrile affording a clear orange solution. To this solution 0.008 g (0.05 mmol) of solid 2,2′-bipyrimidine was added under stirring. Once bpym had completely dissolved after a few minutes, a dark brown solution was obtained. To this solution, 0.036 g (0.1 mmol) of solid $Mn(ClO_4)_2\cdot 6H_2O$ followed by 0.025 g of $Na((CH_3)_3COO)$ (0.2 mmol) were added with vigorous stirring. After 1 h of further stirring the mixture was filtered and the resulting solution left undisturbed slowly evaporating at room temperature. In a few days dark red blocks suitable for X-ray diffraction measurements were obtained. After selecting one specimen for measurement, they were filtered, washed with acetonitrile and vacuum dried (**6**: 0.043 g, 47%). Elemental analysis calcd (%) for **6**, $C_{68}H_{123}Fe_4Mn_2N_4O_{30.5}$: C 44.93, H 6.82, N 3.08; found: C 45.02, H 7.09, N 2.87.

X-Ray structures determination

Crystals suitable for X-ray diffraction were obtained directly from the synthetic procedure for all complexes and mounted in a glass fiber. The crystal structures were determined with a Bruker Smart APEX II CCD area-detector diffractometer using graphite-monochromated Mo Kα radiation (λ = 0.71073 Å) at 173 K. Data was corrected for absorption with SADABS.[43] The structures were solved by direct methods with SHELXS-97 and refined by full-matrix least-squares on F^2 with anisotropic displacement parameters for all non-H atoms with SHELXL-97.[44] Hydrogen atoms were added geometrically and refined as riding atoms with a uniform value of U_{iso} with the exception of hydrogen atoms of coordinated water molecules that were located in the difference map. In all structures, except complex **1**, some pivalate *tert*-butyl groups appeared disordered and were modelled as two split positions with refined occupation factor ratio. Crystallographic data and refinement parameters are shown in Table 1.

DFT quantum computations. Density functional theory (DFT) spin-unrestricted calculations were performed at the X-ray geometry using the Gaussian03 package (revision D.01)[45] at the B3LYP level employing the LanL2DZ basis set. Tightly converged (10^{-8} Eh in energy) single point calculations were performed in order to analyze the exchange coupling between the metallic ion centres. The methodology applied here relies on the broken symmetry formalism, originally developed by Noodleman for SCF methods,[46] which involves a variational treatment within the restrictions of a single spin-unrestricted Slater determinant built upon using different orbitals for different spin. This approach has been later applied within the frame of DFT.[47] The HS (high-spin) and BS (broken symmetry) energies were then combined to estimate the exchange coupling parameter J involved in the widespread used Heisenberg–Dirac–van Vleck Hamiltonian.[48] We have calculated the different spin topologies of broken symmetry nature (see ESI†) by alternatively flipping spin on the different metal sites. The exchange coupling constants J_i can be obtained after considering the individual pair-like components spin interactions involved in the description of the different broken symmetry states. We used two main reported methodologies: the Ising approach,[49] where the broken symmetry states are directly considered as eigenstates of the HDvV Hamiltonian with the corresponding equation:

$$E_{BS} - E_{HS} = 2J_{12}(S_1S_2)$$

and the method proposed by Ruiz and co-workers,[50] where the following equation is applied:

$$E_{BS} - E_{HS} = 2J_{12}(2S_1S_2 + S_2), \text{ with } S_2 < S_1.$$

In both cases a set of linear equations must be solved to obtain the J parameters.

Additionally, we have also employed localized natural orbitals (LNO) with unitary occupancy as a means to visualize the magnetic orbitals and the possible spin-coupling exchange pathways.

Acknowledgements

We gratefully acknowledge the Alexander von Humboldt Foundation for granting a post-doctoral fellowship. We acknowledge Bernd Mienert (MPI-Muelheim) for performing the Mössbauer measurements. This work was partially supported by the National Center for Supercomputing Applications under grant TG-MCA05S010. PA is a member of the Research Staff of CONICET.

References

1 (*a*) A. J. Tasiopoulos, A. Vinslava, W. Wernsdorfer, K. A. Abboud and G. Christou, *Angew. Chem., Int. Ed.*, 2004, **43**, 2117; (*b*) D. Gatteschi and R. Sessoli, *Angew. Chem., Int. Ed.*, 2003, **42**, 268; (*c*) G. Christou, D. Gatteschi, D. N. Hendrickson and R. Sessoli, *MRS Bull.*, 2000, **25**, 66; (*d*) C. J. Milios, A. Vinslava, W. Wernsdorfer, S. Moggach, S. Parsons, S. P. Perlepes, G. Christou and E. K. Brechin, *J. Am. Chem. Soc.*, 2007, **129**, 2754; (*e*) D. Gatteschi, A. Caneschi, L. Pardi and R. Sessoli, *Science*, 1994, **265**, 1054.

2 L. Thomas, F. Lionti, R. Ballou, D. Gatteschi, R. Sessoli and B. Barbara, *Nature*, 1996, **383**, 145.

3 W. Wernsdorfer and R. Sessoli, *Science*, 1999, **284**, 133.

4 (*a*) D. Gatteschi and R. Sessoli, *J. Magn. Magn. Mater.*, 2004, **272–276**, 1030; (*b*) A. Caneschi, D. Gatteschi, C. Sangregorio, R. Sessoli, L. Sorace, A. Cornia, M. A. Novak, C. Paulsen and W. Wernsdorfer, *J. Magn. Magn. Mater.*, 1999, **200**, 182.

5 M. Affronte, *J. Mater. Chem.*, 2009, **19**, 1731.

6 (*a*) L. Bogani and W. Wernsdorfer, *Nat. Mater.*, 2008, **7**, 179; (*b*) M. Cavallini, J. Gomez-Segura, D. Ruiz-Molina, M. Massi, C. Albonetti, C. Rovira, J. Veciana and F. Biscarini, *Angew. Chem., Int. Ed.*, 2005, **44**, 888.

7 (*a*) J. Lehmann, A. Gaita-Arino, E. Coronado and D. Loss, *J. Mater. Chem.*, 2009, **19**, 1672; (*b*) F. Meier, J. Levy and D. Loss, *Phys. Rev. B: Condens. Matter Mater. Phys.*, 2003, **68**, 134417; (*c*) M. N. Leuenberger and D. Loss, *Nature*, 2001, **410**, 789.

8 (*a*) W. Wernsdorfer, *Nat. Nanotechnol.*, 2009, **4**, 145; (*b*) S. Carretta, P. Santini, G. Amoretti, F. Troiani and M. Affronte, *Phys. Rev. B: Condens. Matter Mater. Phys.*, 2007, **76**, 024408.

9 W. Wernsdorfer, N. Aliaga-Alcalde, D. N. Hendrickson and G. Christou, *Nature*, 2002, **416**, 406.

10 (*a*) M. Morimoto, H. Miyasaka, M. Yamashita and M. Irie, *J. Am. Chem. Soc.*, 2009, **131**, 9823; (*b*) L. F. Jones, A. Prescimone, M. Evangelisti and E. K. Brechin, *Chem. Commun.*, 2009, 2023; (*c*) L. Lecren, O. Roubeau, Y. G. Li, X. F. Le Goff, H. Miyasaka, F. Richard, W. Wernsdorfer, C. Coulon and R. Clerac, *Dalton Trans.*, 2008, 755; (*d*) R. Inglis, L. F. Jones, K. Mason, A. Collins, S. A. Moggach, S. Parsons, S. P. Perlepes, W. Wernsdorfer and E. K. Brechin, *Chem.–Eur. J.*, 2008, **14**, 9117; (*e*) L. Lecren, W. Wernsdorfer, Y. G. Li, A. Vindigni, H. Miyasaka and R. Clerac, *J. Am. Chem. Soc.*, 2007, **129**, 5045; (*f*) J. Tao, Y. Z. Zhang, Y. L. Bai and O. Sato, *Inorg. Chem.*, 2006, **45**, 4877; (*g*) H. Miyasaka, K. Nakata, L. Lecren, C. Coulon, Y. Nakazawa, T. Fujisaki, K. Sugiura, M. Yamashita and R. Clerac, *J. Am. Chem. Soc.*, 2006, **128**, 3770; (*h*) L. Lecren, O. Roubeau, C. Coulon, Y. G. Li, X. F. Le Goff, W. Wernsdorfer, H. Miyasaka and R. Clerac, *J. Am. Chem. Soc.*, 2005, **127**, 17353; (*i*) H. Miyasaka, K. Nakata, K. Sugiura, M. Yamashita and R. Clerac, *Angew. Chem., Int. Ed.*, 2004, **43**, 707.

11 (*a*) P. Albores and E. Rentschler, *Inorg. Chem.*, 2008, **47**, 7960; (*b*) Y. Z. Zheng, M. L. Tong, W. Xue, W. X. Zhang, X. M. Chen, F. Grandjean and G. J. Long, *Angew. Chem., Int. Ed.*, 2007, **46**, 6076; (*c*) H. B. Xu, B. W. Wang, F. Pan, Z. M. Wang and S. Gao, *Angew. Chem., Int. Ed.*, 2007, **46**, 7388.

12 S. G. Baca, I. L. Malaestean, T. D. Keene, H. Adams, M. D. Ward, J. Hauser, A. Neels and S. Decurtins, *Inorg. Chem.*, 2008, **47**, 11108.

13 (*a*) G. A. Timco, E. J. L. McInnes, R. G. Pritchard, F. Tuna and R. E. P. Winpenny, *Angew. Chem., Int. Ed.*, 2008, **47**, 9681; (*b*) E. C. Sanudo, T. Cauchy, E. Ruiz, R. H. Laye, O. Roubeau, S. J. Teat and G. Aromi, *Inorg. Chem.*, 2007, **46**, 9045; (*c*) T. Glaser, M. Heidemeier, T. Weyhermuller, R. D. Hoffmann, H. Rupp and P. Muller, *Angew. Chem., Int. Ed.*, 2006, **45**, 6033; (*d*) H. J. Eppley, N. deVries, S. Y. Wang, S. M. Aubin, H. L. Tsai, K. Folting, D. N. Hendrickson and G. Christou, *Inorg. Chim. Acta*, 1997, **263**, 323; (*e*) V. A. Grillo, M. J. Knapp, J. C. Bollinger, D. N. Hendrickson and G. Christou, *Angew. Chem., Int. Ed. Engl.*, 1996, **35**, 1818; (*f*) S. Wang, H. L. Tsai, K. Folting, J. D. Martin, D. N. Hendrickson and G. Christou, *J. Chem. Soc., Chem. Commun.*, 1994, 671.

14 G. A. Timco, S. Carretta, F. Troiani, F. Tuna, R. J. Pritchard, C. A. Muryn, E. J. L. McInnes, A. Ghirri, A. Candini, P. Santini, G. Amoretti, M. Affronte and R. E. P. Winpenny, *Nat. Nanotechnol.*, 2009, **4**, 173.

15 R. D. Cannon and R. P. White, *Prog. Inorg. Chem.*, 1988, **36**, 195.

16 R. Sessoli, H. L. Tsai, A. R. Schake, S. Y. Wang, J. B. Vincent, K. Folting, D. Gatteschi, G. Christou and D. N. Hendrickson, *J. Am. Chem. Soc.*, 1993, **115**, 1804.

17 A. S. Lytvynenko, S. V. Kolotilov, O. Cador, K. S. Gavrilenko, S. Golhen, L. Ouahab and V. V. Pavlishchuk, *Dalton Trans.*, 2009, 3503.

18 (*a*) S. T. Wilson, R. F. Bondurant, T. J. Meyer and D. J. Salmon, *J. Am. Chem. Soc.*, 1975, **97**, 2285; (*b*) T. Ito, T. Hamaguchi, H. Nagino, T. Yamaguchi, J. Washington and C. P. Kubiak, *Science*, 1997, **277**, 660; (*c*) T. Yamaguchi, N. Imai, T. Ito and C. P. Kubiak, *Bull. Chem. Soc. Jpn.*, 2000, **73**, 1205; (*d*) H. E. Toma, K. Araki, A. D. P. Alexiou, S. Nikolaou and S. Dovidauskas, *Coord. Chem. Rev.*, 2001, **219–221**, 187; (*e*) R. J. Crutchley, *Angew. Chem., Int. Ed.*, 2005, **44**, 6452.

19 R. A. Reynolds, W. R. Dunham and D. Coucouvanis, *Inorg. Chem.*, 1998, **37**, 1232.

20 K. S. Gavrilenko, A. Vertes, G. Vanko, L. F. Kiss, A. W. Addison, T. Weyhermuller and V. V. Pavlishchuk, *Eur. J. Inorg. Chem.*, 2002, 3347.

21 (*a*) T. Nakamoto, M. Hanaya, M. Katada, K. Endo, S. Kitagawa and H. Sano, *Inorg. Chem.*, 1997, **36**, 4347; (*b*) H. G. Jang, K. Kaji, M. Sorai, R. J. Wittebort, S. J. Geib, A. L. Rheingold and D. N. Hendrickson, *Inorg. Chem.*, 1990, **29**, 3547.

22 S. Shova, D. Prodius, V. Mereacre, Y. A. Simonov, J. Lipkowski and C. Turta, *Inorg. Chem. Commun.*, 2004, **7**, 292.

23 T. Sato and F. Ambe, *Acta Crystallogr., Sect. C: Cryst. Struct. Commun.*, 1996, **52**, 3005.

24 (*a*) S. G. Baca, I. G. Filippova, C. Ambrus, M. Gdaniec, Y. A. Simonov, N. Gerbeleu, O. A. Gherco and S. Decurtins, *Eur. J. Inorg. Chem.*, 2005, 3118; (*b*) X. X. Hu, J. Q. Xu, P. Cheng, X. Y. Chen, X. B. Cui, J. F. Song, G. D. Yang and T. G. Wang, *Inorg. Chem.*, 2004, **43**, 2261; (*c*) A. Grirrane, A. Pastor, A. Ienco, C. Mealli and A. Galindo, *J. Chem. Soc., Dalton Trans.*, 2002, 3771; (*d*) M. J. Plater, M. R. S. Foreman, E. Coronado, C. J. Gomez-Garcia and A. M. Z. Slawin, *J. Chem. Soc., Dalton Trans.*, 1999, 4209; (*e*) J. Cano, G. DeMunno, J. L. Sanz, R. Ruiz, J. Faus, F. Lloret, M. Julve and A. Caneschi, *J. Chem. Soc., Dalton Trans.*, 1997, 1915; (*f*) O. F. Ikotun, W. Ouellette, F. Lloret, M. Julve and R. P. Doyle, *Eur. J. Inorg. Chem.*, 2007, 2083; (*g*) Y. G. Li, N. Hao, Y. Lu, E. B. Wang, Z. H. Kang and C. W. Hu, *Inorg. Chem.*, 2003, **42**, 3119; (*h*) S. B. Jedner, H. Schwoppe, H. Nimir, A. Rompel, D. A. Brown and B. Krebs, *Inorg. Chim. Acta*, 2002, **340**, 181; (*i*) I. L. Eremenko, S. E. Nefedov, A. A. Sidorov, M. A. Golubnichaya, P. V. Danilov, V. N. Ikorskii, Y. G. Shvedenkov and V. M. Novotortsev, Moiseev, II, *Inorg. Chem.*, 1999, **38**, 3764; (*j*) R. C. Holz, E. A. Evdokimov and F. T. Gobena, *Inorg. Chem.*, 1996, **35**, 3808.

25 (*a*) A. K. Boudalis, V. Tangoulis, C. P. Raptopoulou, A. Terzis, J. P. Tuchagues and S. P. Perlepes, *Inorg. Chim. Acta*, 2004, **357**, 1345; (*b*) A. K. Boudalis, N. Lalioti, G. A. Spyroulias, C. P. Raptopoulou, A. Terzis, A. Bousseksou, V. Tangoulis, J. P. Tuchagues and S. P. Perlepes, *Inorg. Chem.*, 2002, **41**, 6474; (*c*) A. K. Boudalis, N. Lalioti, G. A. Spyroulias, C. P. Raptopoulou, A. Terzis, V. Tangoulis and S. P. Perlepes, *J. Chem. Soc., Dalton Trans.*, 2001, 955; (*d*) J. M. Vincent, S. Menage, J. M. Latour, A. Bousseksou, J. P. Tuchagues, A. Decian and M. Fontecave, *Angew. Chem., Int. Ed. Engl.*, 1995, **34**, 205.

26 P. Albores and E. Rentschler, *Dalton Trans.*, 2009, 2609.

27 (*a*) F. Thetiot, S. Triki, J. S. Pala, J. R. Galan-Mascaros, J. M. Martinez-Agudo and K. R. Dunbar, *Eur. J. Inorg. Chem.*, 2004, 3783; (*b*) S. R.

Marshall, C. D. Incarvito, J. L. Manson, A. L. Rheingold and J. S. Miller, *Inorg. Chem.*, 2000, **39**, 1969.
28 (*a*) G. De Munno, T. Poerio, M. Julve, F. Lloret and G. Viau, *New J. Chem.*, 1998, **22**, 299; (*b*) G. Demunno, M. Julve, F. Lloret, J. Faus and A. Caneschi, *J. Chem. Soc., Dalton Trans.*, 1994, 1175; (*c*) G. Demunno, M. Julve, F. Lloret and A. Derory, *J. Chem. Soc., Dalton Trans.*, 1993, 1179.
29 (*a*) G. Brewer and E. Sinn, *Inorg. Chem.*, 1985, **24**, 4580; (*b*) E. Colacio, F. Lloret, M. Navarrete, A. Romerosa, H. Stoeckli-Evans and J. Suarez-Varela, *New J. Chem.*, 2005, **29**, 1189; (*c*) S. Martin, M. G. Barandika, R. Cortes, J. I. R. de Larramendi, M. K. Urtiaga, L. Lezama, M. I. Arriortu and T. Rojo, *Eur. J. Inorg. Chem.*, 2001, 2107.
30 G. De Munno, W. Ventura, G. Viau, F. Lloret, J. Faus and M. Julve, *Inorg. Chem.*, 1998, **37**, 1458.
31 (*a*) A. K. Boudalis, Y. Sanakis, C. P. Raptopoulou and V. Psycharis, *Inorg. Chim. Acta*, 2007, **360**, 39; (*b*) A. K. Boudalis, Y. Sanakis, C. P. Raptopoulou, A. Terzis, J. P. Tuchagues and S. P. Perlepes, *Polyhedron*, 2005, **24**, 1540; (*c*) J. Overgaard, E. Rentschler, G. A. Timco, N. V. Gerbeleu, V. Arion, A. Bousseksou, J. P. Tuchagues and F. K. Larsen, *J. Chem. Soc., Dalton Trans.*, 2002, 2981; (*d*) R. W. Wu, M. Poyraz, F. E. Sowrey, C. E. Anson, S. Wocadlo, A. K. Powell, U. A. Jayasooriya, R. D. Cannon, T. Nakamoto, M. Katada and H. Sano, *Inorg. Chem.*, 1998, **37**, 1913.
32 B. S. Tsukerblat, A. V. Palii, V. Y. Mirovitskii, S. M. Ostrovsky, K. Turta, T. Jovmir, S. Shova, J. Bartolome, M. Evangelisti and G. Filoti, *J. Chem. Phys.*, 2001, **115**, 9528.
33 (*a*) J. Krzystek, A. Ozarowski and J. Telser, *Coord. Chem. Rev.*, 2006, **250**, 2308; (*b*) R. Boca, *Coord. Chem. Rev.*, 2004, **248**, 757.
34 (*a*) G. DeMunno, M. Julve, G. Viau, F. Lloret, J. Faus and D. Viterbo, *Angew. Chem., Int. Ed. Engl.*, 1996, **35**, 1807; (*b*) G. DeMunno, G. Viau, M. Julve, F. Lloret and J. Faus, *Inorg. Chim. Acta*, 1997, **257**, 121; (*c*) D. Armentano, G. de Munno, F. Guerra, J. Faus, F. Lloret and M. Julve, *Dalton Trans.*, 2003, 4626; (*d*) N. Marino, T. F. Mastropietro, D. Armentano, G. De Munno, R. P. Doyle, F. Lloret and M. Julve, *Dalton Trans.*, 2008, 5152.
35 O. Fabelo, J. Pasan, F. Lloret, M. Julve and C. Ruiz-Perez, *Inorg. Chem.*, 2008, **47**, 3568.
36 J. J. Borras-Almenar, J. M. Clemente-Juan, E. Coronado and B. S. Tsukerblat, *J. Comput. Chem.*, 2001, **22**, 985.
37 (*a*) P. Albores and E. Rentschler, *Eur. J. Inorg. Chem.*, 2008, 4004; (*b*) P. Albores and E. Rentschler, *Polyhedron*, 2009, **28**, 1912.
38 M. Julve, G. Demunno, G. Bruno and M. Verdaguer, *Inorg. Chem.*, 1988, **27**, 3160.
39 A. M. Bond, R. J. H. Clark, D. G. Humphrey, P. Panayiotopoulos, B. W. Skelton and A. H. White, *J. Chem. Soc., Dalton Trans.*, 1998, 1845.
40 G. Aromi, A. S. Batsanov, P. Christian, M. Helliwell, A. Parkin, S. Parsons, A. A. Smith, G. A. Timco and R. E. P. Winpenny, *Chem.–Eur. J.*, 2003, **9**, 5142.
41 G. Chaboussant, R. Basler, H. U. Gudel, S. Ochsenbein, A. Parkin, S. Parsons, G. Rajaraman, A. Sieber, A. A. Smith, G. A. Timco and R. E. P. Winpenny, *Dalton Trans.*, 2004, 2758.
42 G. Vlad and I. T. Horvath, *J. Org. Chem.*, 2002, **67**, 6550.
43 G. M. Sheldrick, *SADABS, Program for area detector adsorption correction*, Institute for Inorganic Chemistry, University of Göttingen, Germany, 1996.
44 G. M. Sheldrick, *SHELXL-97, Program for refinement of crystal structures*, University of Göttingen, Germany, 1997; G. M. Sheldrick, *SHELXS-97, Program for solution of crystal structures*, University of Göttingen, Germany, 1997.
45 M. J. Frisch, G. W. Trucks, H. B. Schlegel, G. E. Scuseria, M. A. Robb, J. R. Cheeseman, J. A. Montgomery, Jr., T. Vreven, K. N. Kudin, J. C. Burant, J. M. Millam, S. S. Iyengar, J. Tomasi, V. Barone, B. Mennucci, M. Cossi, G. Scalmani, N. Rega, G. A. Petersson, H. Nakatsuji, M. Hada, M. Ehara, K. Toyota, R. Fukuda, J. Hasegawa, M. Ishida, T. Nakajima, Y. Honda, O. Kitao, H. Nakai, M. Klene, X. Li, J. E. Knox, H. P. Hratchian, J. B. Cross, V. Bakken, C. Adamo, J. Jaramillo, R. Gomperts, R. E. Stratmann, O. Yazyev, A. J. Austin, R. Cammi, C. Pomelli, J. Ochterski, P. Y. Ayala, K. Morokuma, G. A. Voth, P. Salvador, J. J. Dannenberg, V. G. Zakrzewski, S. Dapprich, A. D. Daniels, M. C. Strain, O. Farkas, D. K. Malick, A. D. Rabuck, K. Raghavachari, J. B. Foresman, J. V. Ortiz, Q. Cui, A. G. Baboul, S. Clifford, J. Cioslowski, B. B. Stefanov, G. Liu, A. Liashenko, P. Piskorz, I. Komaromi, R. L. Martin, D. J. Fox, T. Keith, M. A. Al-Laham, C. Y. Peng, A. Nanayakkara, M. Challacombe, P. M. W. Gill, B. G. Johnson, W. Chen, M. W. Wong, C. Gonzalez and J. A. Pople, *GAUSSIAN 03 (Revision D.01)*, Gaussian, Inc., Wallingford, CT, 2004.
46 L. Noodleman, *J. Chem. Phys.*, 1981, **74**, 5737.
47 L. Noodleman and E. J. Baerends, *J. Am. Chem. Soc.*, 1984, **106**, 2316.
48 O. Kahn, *Molecular Magnetism*, VCH, New York, 1993.
49 D. D. Dai and M. H. Whangbo, *J. Chem. Phys.*, 2003, **118**, 29.
50 E. Ruiz, A. Rodriguez-Fortea, J. Cano, S. Alvarez and P. Alemany, *J. Comput. Chem.*, 2003, **24**, 982.